Geochemistry, Geophysics, Geosystems®

RESEARCH ARTICLE
10.1029/2021GC009833

Landslides in the Upper Submarine Slopes of Volcanic Islands: The Central Azores

Yu-Chun Chang[1], Neil C. Mitchell[1], and Rui Quartau[2,3]

[1]Department of Earth and Environmental Sciences, University of Manchester, Manchester, UK, [2]Divisão de Geologia Marinha, Instituto Hidrográfico, Lisboa, Portugal, [3]Instituto Dom Luiz, Faculdade de Ciências da Universidade de Lisboa, Lisboa, Portugal

Key Points:

- Submarine slope landslide area and volume follow log-normal probability density functions
- Landslide area and volume are markedly different between the islands, potentially a result of different long-term seismicity
- Some landslides potentially generate tsunamis >1 m at source, which are hazardous due to short travel distances and recurrence intervals

Supporting Information:

Supporting Information may be found in the online version of this article.

Correspondence to:

Y.-C. Chang,
yu-chun.chang@manchester.ac.uk

Citation:

Chang, Y.-C., Mitchell, N. C., & Quartau, R. (2021). Landslides in the upper submarine slopes of volcanic islands: The central Azores. *Geochemistry, Geophysics, Geosystems*, *22*, e2021GC009833. https://doi.org/10.1029/2021GC009833

Received 4 MAY 2021
Accepted 5 SEP 2021

Abstract Small landslides in the upper submarine slopes of volcanic islands present potential hazards locally because of their high frequency. We examine evidence for landsliding in high-resolution bathymetric data from Faial, Pico, São Jorge, and Terceira islands of the Azores. Because the rugged morphology of the upper slopes makes landslides difficult to interpret, we develop two classification schemes for the 1,227 identified slope valleys. One scheme addresses how recognizable the valleys were as originating from landslides (whether scarps are prominent or indefinite), whereas the other scheme addresses valley types (whether apparently produced by single or multiple failures). Size distributions are used to assess the relative occurrence of large versus small landslides. Thirteen landslides are predicted to have generated tsunami heights at source of >1 m and one with height of >7 m. Some slopes have gradients far above 30°, the angle of repose of incohesive clastic sediment, so the seabed in those areas is strengthened perhaps by carbonate cementation, by seismic shaking or by the presence of coherent lava or lava talus. Using all types of slope valleys, Faial and Pico have smaller affected volumes per unit slope area than those of São Jorge and Terceira. These differences could be associated with varied seismic activity, with more frequent earthquakes beneath Faial and Pico preventing the build-up of sediments on their slopes. Submarine landslide statistics are therefore potentially useful for assessing long-term earthquake hazards of volcanic islands in seismically active environments such as the Azores.

Plain Language Summary Many valleys are found in the underwater slopes of volcanic islands, and some of them are likely caused by submarine landslides. If such landslides were to occur today, they could generate tsunamis threatening local coasts. This research assesses such landslides in the Azores based mainly on high-resolution echo-sounder data. It illustrates methods that are potentially repeatable at other volcanic islands with suitable data. More than 1,200 submarine valleys have been mapped. Thirteen of them would likely have generated tsunamis above the landslides with heights between 1 and 7 m, and hence potentially hazardous. Valleys produced by landslides around Faial and Pico islands are generally smaller than those around São Jorge and Terceira islands. These differences could be associated with more frequent earthquakes beneath Faial and Pico, which prevent the build-up of thick sediment on their submarine slopes needed for large landslides. Studies of landslide occurrences around volcanic islands could therefore be useful to assess threats of tsunamis and earthquakes where these are not well documented by other methods.

1. Introduction

Giant landslides have been found around many volcanic ocean islands (those located away from convergent margins), including the Canary archipelago (Masson et al., 2002, 2006; Mitchell et al., 2002; Wynn & Masson, 2003), the Hawaiian Islands (Lipman et al., 1988; McMurtry et al., 2004; Moore et al., 1989, 1994), Cape Verdes (Barrett et al., 2019; Masson et al., 2008; Ramalho et al., 2015), Madeira archipelago (Quartau et al., 2018; Santos et al., 2019), Reunion Island (Labazuy, 1996; Ollier et al., 1998), and islands near mid-ocean ridges (Mitchell, 2003). Smaller submarine landslides have been found in the steep upper flanks of volcanic islands and they have generated tsunamis (Alberico et al., 2018; Casalbore et al., 2011, 2018; Casas et al., 2016; Chiocci et al., 2008; Fornaciai et al., 2019; Kelfoun et al., 2010; Rahiman & Pettinga, 2006; Tinti et al., 2005; Tommasi et al., 2008), but their threats are less well known. These smaller landslides are more frequent (Casalbore et al., 2011; Chiocci & Casalbore, 2017) compared with the giant landslides, which recur globally every ~10 Kyr around volcanic islands and locally every >100 Kyr in the Canary (Krastel

et al., 2001) and Hawaiian Islands (Garcia et al., 2006). Although tsunamis they generate are smaller, those tsunamis may nevertheless be significant geohazards because of their greater frequency. According to historical reports analyzed by Andrade et al. (2006), at least 23 tsunamis have affected the Azores since the human settlement of the islands and one with wave height >10 m. Some of them were not explained by earthquakes so they may have originated from submarine landslides. One motivation for this research was therefore to investigate the sizes and geometries of upper-slope submarine landslides among the islands, in order to assess whether the landslides were large enough to generate tsunamis.

Earthquakes also pose significant geohazards on volcanic ocean islands and can include events of magnitude $M > 7.0$ (Crossen & Endo, 1982; Furumoto & Kovach, 1979; Madeira et al., 2015). Unfortunately, the instrumental record is not sufficient to characterize seismic hazards of small areas (Scholz, 2002). As the central and eastern Azores islands lie in a region of distributed deformation of the Eurasia-Nubia plate boundary (Lourenço et al., 1998; Figure 1), they are seismically active. The question of adequacy of the instrumental record is, therefore, important locally. In particular, onshore mapping and sonar data has revealed potentially active faults of 10–20 km in length (Casalbore et al., 2015; Lourenço et al., 1998; Madeira et al., 2015; Mitchell et al., 2012), whereas the north slope of São Jorge, which appears fault controlled (Walker, 1999), is 60 km long and the walls of the Terceira Rift (Figure 1a) reach 100 km in length. Madeira et al. (2015) estimated that earthquakes up to $M = 6.8$ could occur based on the lengths of active faults mapped on the islands, but this is likely an underestimate as the submarine faults are longer. From data compiled by Scholz (1994), a strike-slip rupture of 110 km length (the approximate maximum of the faults outlined later) could produce an earthquake with seismic moment $\sim 5 \times 10^{20}$ N m (i.e., moment magnitude $Mw \sim 7.4$). Such an earthquake would be similar in size to events that have occurred in the Azores historically (e.g., $Mw \sim 7.2$; Gaspar et al., 2015). If such a large event were to occur in the Azores, its effects would be exacerbated by the poor preparedness of legacy buildings (Maio et al., 2017). Unfortunately, assessing the frequency of large earthquakes is difficult because paleoseismological methods are not easily applied to volcanic sequences and many of the faults lie underwater. Alternative assessment methods are therefore needed.

High-resolution bathymetric data have revealed evidence of widespread submarine mass wasting along the upper submarine slopes of islands in the Azores (Mitchell et al., 2008, 2012; Quartau et al., 2012, 2014, 2015; Ricchi et al., 2020). Unfortunately, those data such as shown in Figures 1b–1e present a difficulty of interpretation. Whereas landslides in continental slopes often occur over decollements parallel to the seabed and create landslide scars that are clearly defined (e.g., ten Brink et al., 2006), this is not the case in the Azores data, which instead show a rugged morphology likely due to past volcanic history, transfer of slope sediments and multiple small-scale landsliding. We address this problem by adopting the general term "slope valley" for topographic depressions without connotations of origin. Within a database of such identified features, we classify them first according to the degree to which they adhere to the classical features of landslides (Varnes, 1978). A second classification is then used to separate them according to whether they appear to form single landslide scars, amphitheaters created by multiple landslide events (e.g., Pratson & Coakley, 1996) or potential retrogressive failures. We then interrogate this database using the different classes depending on the objective being addressed. The results indicate a significant variation in submarine slope landsliding and hence hazard among the islands.

2. Geological Setting

It is useful to know aspects of Azorean geology in order to assess how frequently volcanic materials are fed to the coasts during eruptions and earthquakes, both of which may affect landslide frequency and geomorphology. The central Azores islands of Faial, Pico, São Jorge, Graciosa, and Terceira lie east of the Mid-Atlantic Ridge (Figure 1). Rift zones, faults on land and submarine ridges commonly lie perpendicular or oblique to Nubia-Eurasia plate motion suggesting that they were produced by trans-tensional deformation, continuing through the Quaternary to the present-day (Lourenço et al., 1998; Madeira & Brum da Silveira, 2003). Recent $^{40}Ar/^{39}Ar$ and K/Ar dating results suggest that Terceira is generally young, with the earliest-formed edifice in the east younger than 0.4 Ma and the most recent edifice in the west ~50 ka (Calvert et al., 2006; Hildenbrand et al., 2014). São Jorge Island can be subdivided into old and young volcanic complexes (Figure 1). The oldest complex in the southeast is 1.2–1.85 Ma and the intermediate

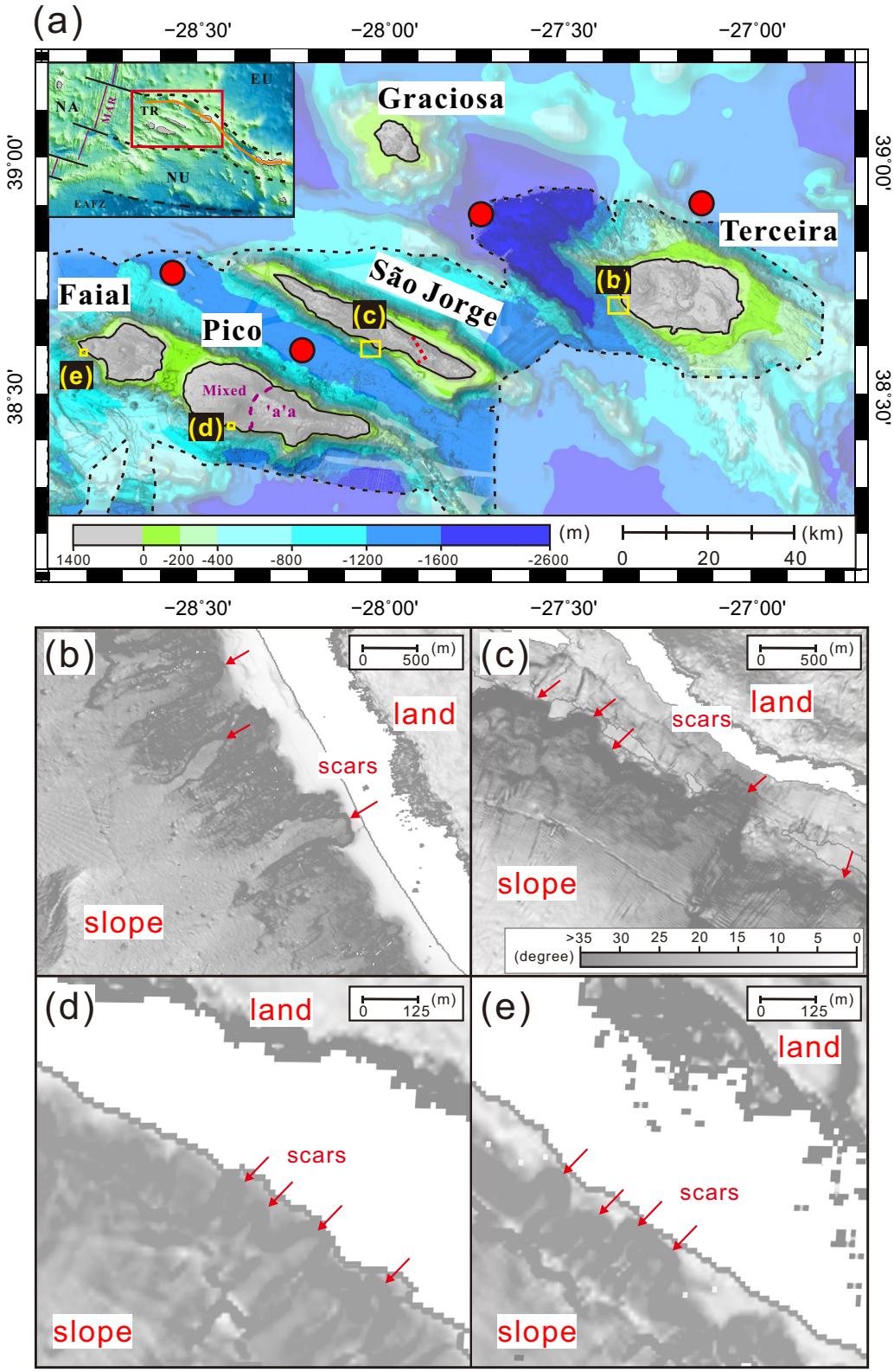
(a)
−28°30'
−28°00'
−27°30'
−27°00'
39°00'
38°30'
EU
NA
MAR
TR
NU
EAFZ
Graciosa
Terceira
São Jorge
Faial
Pico
(b)
(c)
(d)
(e)
Mixed
'a'a
(m)
(km)
1400
0
-200
-400
-800
-1200
-1600
-2600
0
20
40
(b)
land
scars
slope
0
500
(m)
(c)
land
scars
slope
>35
30
25
20
15
10
5
0
(degree)
(d)
land
scars
slope
0
125
(m)
(e)
land
scars
slope
0
125
(m)

Figure 1.

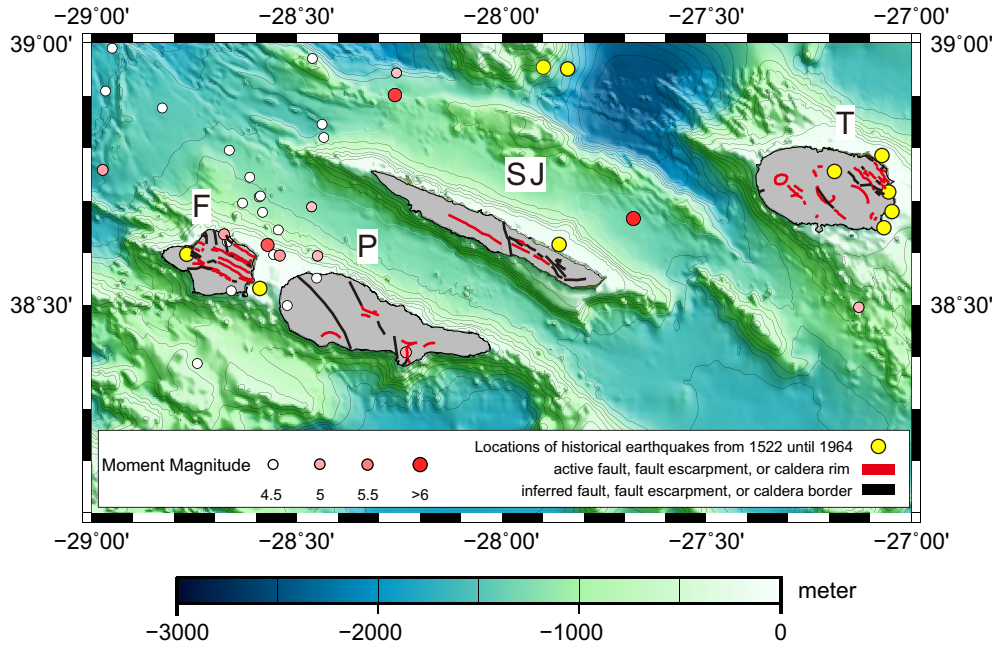

Figure 2. Distributions of earthquakes. Earthquakes shown with moment magnitude scaling were recorded between 1964 and 2019 and were derived from the International Seismological Centre catalog (*Mw* > 4.5 shown). Yellow circles locate historical earthquakes from 1522 until 1964 (Gaspar et al., 2015, their Table 4-1). Red and black lines represent active and inferred faults on land, respectively (Madeira et al., 2015). F, P, SJ, and T are Faial, Pico, São Jorge, and Terceira, respectively.

to young volcanic complex in the northwest is younger than 0.75 Ma based on $^{40}Ar/^{39}Ar$ and K/Ar dating (Hildenbrand et al., 2008; Marques et al., 2018; Pinto Ribeiro et al., 2010). The northwest of São Jorge also has had historical eruptions in 1580 and 1808 (Madeira, 1998). Although K/Ar dates suggest the maximum age for Faial Island is 0.85 Ma (Hildenbrand et al., 2012), most parts of the island are widely blanketed by a 10–440 ka volcanic complex (Pacheco, 2002; Pimentel et al., 2015). The youngest part of Faial in the west (<10 ka) also experienced the historical Capelinhos eruption in 1957/58 (Machado et al., 1962). K/Ar dates suggest an oldest age of 0.19 Ma for Pico Island (Costa et al., 2015), which has had three historical eruptions since 1562. Lava flows of Pico volcano in the west of the island originated from the summit area and some from flank sources. The flows include both pahoehoe and 'a'a lava types. In contrast, 'a'a lava flows are more common in eastern Pico (Figure 1; Scarth & Tanguy, 2001).

Neotectonic structures (Figure 2) can be explained by regional trans-tension (Lourenço et al., 1998). Active strike-slip faults on São Jorge and Pico islands are revealed by sheared cinder cones (Madeira & Brum da Silveira, 2003). Some Holocene lava flows have been displaced by faults (Madeira et al., 2015), which is evidence of pre-historic seismic activity. From 1522 to 1964, at least 10 destructive earthquakes occurred in the central Azores (Figure 2) responsible for hundreds of deaths (Gaspar et al., 2015). Since 1980, seismometers have been installed on several Azores islands (CIVISA, 1998), greatly improving earthquake detection threshold and location accuracy (Carvalho et al., 2001). At least 30 earthquakes of *Mw* > 4.5 were recorded (Figure 2).

Figure 1. (a) Distribution of high-resolution bathymetry data in the central Azores available to this study (outlined by black-dashed lines). Red dashed line on São Jorge Island is the boundary separating the old volcanic complex in the southeast from the young volcanic complex in the northwest. Purple dashed line on Pico Island is the boundary separating 'a'a lava flow dominated zone of Pico Mountain from the zone of mixed lava types i the east of the island. Background bathymetric data are from Ryan et al. (2009). Island elevations above sea-level are shown in gray with black outlines. Red circles locate the sediment cores analyzed by Chang et al. (2021). Inset shows the regional tectonic setting of the area in the diffuse boundary between the Eurasia (EU) and Nubia (NU) plates (NA: North American plate). Purple lines locate the Mid-Atlantic Ridge (MAR), solid black lines locate its associated fracture zones, and dashed-dot-dashed line locates the East Azores Fracture Zone (EAFZ). Dashed black lines are the limits of the diffuse Nu-Eu plate boundary and the orange solid line represents the center of Terceira Rift (TR). (b–e) Selected maps of maximum local gradient revealing landslide scars in the steep upper island submarine slopes. Map extents are shown by yellow rectangles in (a). The gradients in these four panels share the scale in (c). Red arrows locate interpreted landslide scars.

The deposits forming the upper submarine slopes have not been directly observed or sampled, but their origins can be speculated on. Quartau et al. (2012, 2015) showed that the shelves of the Azores islands have recently been accumulating volcaniclastic particles from subaerial and coastal erosion and carbonate particles from in situ biogenic production. Such sediments likely accumulated since the Last Glacial Maximum and are generally only 10 ms thick, although a seismic reflection image in Marques et al. (2018, their Figure 8) reveals an unusually thick 250 ms (~225 m) of sediment in the outer shelf of northeast São Jorge. During sea-level lowerings, such sediments are likely to be remobilized by coastal and subaerial erosion, and some of those sediments redeposited in the upper submarine slopes. Sonar images of the shelves of Pico and Faial reveal Holocene dendritic lava flows, lobes and deltas (Mitchell et al., 2008; Quartau et al., 2012, 2015). During sea-level low-stands, seaward extending shorelines probably allowed such lava flows to reach the outer shelves and hence feed the uppermost slopes. Sedimentary particles released by erosion by streams and waves also likely fed the upper submarine slopes of the islands at such times. However, during sea-level high-stands, sediment can also be produced and exported from shelves due to greater biogenic production (Droxler & Schlager, 1985). It is presently unclear exactly how the flux of sediment to the island slopes has varied over time.

Offshore sediment gravity cores have been collected around these islands, which contain turbidites likely originating from slope landslides such as those we describe here. Analyses of four of those cores located in Figure 1 (Chang et al., 2021) has revealed that those turbidites comprise mainly silt to sand grade volcaniclastic and minor bioclastic particles. Glass shard analysis and other data suggest that more than half of the turbidites originated as primary volcaniclastic events (i.e., pyroclastic flows). Much of the uppermost slopes of the islands may therefore also include such volcaniclastic deposits.

3. Materials and Methods

3.1. Research Materials

High-resolution bathymetric data were collected on RV *Arquipélago* in 2003 and RV *l'Atalante* in 2011, providing the coverage outlined in Figure 1. The *Arquipélago* survey was carried out with a portable multibeam sonar (Mitchell et al., 2008) and covered the submarine slopes of Faial, Pico and São Jorge islands. These data suffer from imperfect rigidity of the transducer mounting, which led to an artificial high-frequency cross-track corrugation of the data, which needs to be borne in mind in interpretation (e.g., in the class C example in Figure 2). The 2011 survey was carried out during project Features of Azores and Italian Volcanic Islands (FAIVI). Bathymetry data were collected around Terceira Island, with a survey boat deployed into coastal areas. Those combined data have a resolution of ~1 m in the first 100 m water depth increasing to 50 m at 2,000 m depths (Casalbore et al., 2015; Chiocci et al., 2013; Quartau et al., 2014).

The earthquake event data were acquired from the International Seismological Centre (ISC) un-reviewed catalog for the years 1964–2019. Figure 2 shows the 30 largest earthquakes with $Mw > 4.5$. Historical earthquakes from 1522 until 1964 are from Gaspar et al. (2015) and the locations and lengths of active and inferred faults on land are from Madeira et al. (2015).

3.2. Landslide Identification and Calculations of Area and Volume

An idealized landslide comprises both an embayment or scar created by removed material and an emplaced mound of deposits, sometimes also with a chute in between (Clare et al., 2018; Hampton et al., 1996). Slope valleys that are potential landslide scars were identified by inspecting multiple perspective views of the shaded bathymetric data and seafloor gradient maps, also using tightly spaced contour lines as an indicator of steep gradients. Given the varied data resolutions and poor imaging at deep water depths where the deposits lie, mapping complete landslides was considered to be unrealistic. Therefore, our mapping focused on the heads of landslides only. Even with this focus, subjective decisions were necessary because some headwall escarpments are variably reworked or obscured by later sedimentation. Moreover, headwalls and boundaries between adjacent valleys can become obscured by subsequent slope failures and some escarpments appeared likely formed from multiple events.

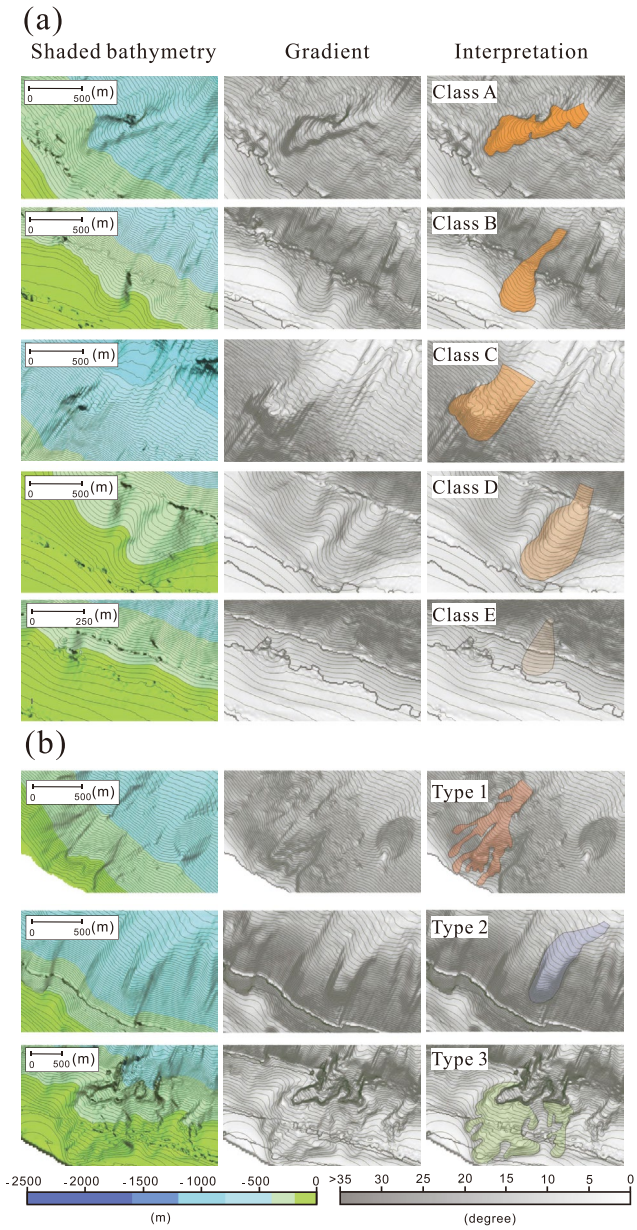

Figure 3. Illustration of different classes and types of valley polygons. Contour interval is 10 m. (a) Classes based on recognition as landslides with A the most recognizable as landslide scars, E the least recognizable as such. (b) Classification based on suspected number of failure events. Type 1 contains multiple branches, suggesting multiple failures. Type 2 contains a single prominent valley, likely created by a single failure. Type 3 contains a valley lying above a prominent escarpment, which potentially developed by retrogressive failure, either during or after the lower failure.

The slope valleys were classified in two ways (Figure 3; see detailed mapping results in Supporting Information S1). The first classification addresses the varied level of recognition of these features as landslides and hence conveys our confidence in their landslide origins. The second classification addresses whether their morphologies suggest they formed by single slope failure events or by multiple events (either subsequent different events or retrogressive failures occurring over finite periods). For the recognition classification, five classes (A–E) were chosen as follows (Figure 3a). Class A: headwalls and sidewalls can be clearly identified by sharp gradient changes and commonly with significant depth changes. Class B: headwalls and sidewalls mostly can be identified by sharp gradient changes and commonly with significant depth changes, though parts of them are less well defined. Class C: headwalls can be mostly identified from gradient changes but sidewalls are obscured or missing. Class D: headwalls and sidewalls are delineated based on modest gradient and depth changes (valleys belonging to this class commonly still have a depression). Class E: headwalls and sidewalls are delineated based on mild gradient and depth changes.

Examples illustrating our second classification scheme are shown in Figure 3b. The slope valleys were subdivided into three types (1–3) based on their morphometric features. Type 1 valleys were interpreted as produced by multiple failure events. In this cases, multiple-branching valleys were identified and each of them appears important. Later erosive features can also overprint the main rupture surface. Type 2 valleys were interpreted as each produced by a single major failure event. Each valley contains a prominent headscarp. Type 3 valleys lie above the headscarps of type 1 or 2 valleys, so we interpreted them as the result of retrogressive failures. They have gentler gradients and form depressions of the sediment surface. Although those depressions could be artifacts, such as due to sediment aggradation around them or other factors, landsliding has occurred in similar shallow gradients and layered carbonate-rich deposits (Schwab et al., 1988), so we suggest these were potentially also earthquake-triggered failures. Type 3 valleys typically occur in the outermost shelves of the islands, which are fully mapped in the multibeam data.

The areas and volumes of valleys were measured following the methods of ten Brink et al. (2006). We first manually digitized the boundary of each valley encompassing the potentially collapsed region to acquire valley area. We then created a smooth upper surface by interpolating over the perimeter of each digitized polygon. The present-day bathymetry (lower surface) was then subtracted from the interpolated surface (upper surface) to acquire valley volume. As the investigated submarine slope area varies amongst the islands and hence also affects the abundances of landslide valleys, we normalized landslide valley areas and volumes by dividing them by the submarine slope areas.

These measurements have the following potential uncertainties. (1) Later sediments deposited in slope valleys bias volume estimates. (2) Further erosion may be possible from sediment movements during or shortly following each slope failure. (3) Oblique artifacts due to the non-rigid mounting of the 2003 data can influence the topography of headscarps. Uncertainty (3) is minimized, as most slope valleys were located in the upper slopes. We mitigate against uncertainty (1) when assessing tsunami risks by only studying the more distinct landslide scars (classes A–C and type 2). That uncertainty may affect our inter-island comparisons of landslide volume, although we also check variations using scars with prominent scarps. Uncertainty (2)

can potentially also affect the landslide volumes (e.g., Sun et al., 2018). However, the variations in landslide volumes can be verified if similar variations also occur in the landslide areas, which are less affected by either depositional or erosional modifications. Furthermore, our results below suggest that the material has significant cohesion and is thus more resistant to erosions by small sedimentary flows in the uppermost island slopes.

3.3. Landslide Size-Frequency Analysis

The complementary cumulative distribution function (CCDF) has been used to represent the probability that a landslide greater than a particular size will occur and is helpful for summarizing the distribution of landslide sizes as it emphases the larger features (e.g., Malamud et al., 2004). CCDFs of area and volume were generated from slope valleys best representing single-event landslide scars (classes A-C and type 2). Their correspondence with models (goodness-of-fit) was tested using Kolmogorov-Smirnov test (K-S test) and the *p*-value suggested by Clauset et al. (2009). The K-S test is a nonparametric test of the equality of continuous or discontinuous variations. It is used to quantify an interval between the empirical cumulative distribution function of the sample and the reference distribution. The *p*-value can vary from 0 to 1. If it is higher than 0.1, the observed data fit the tested distribution, whereas a *p*-value equal to or less than 0.1 suggests that the data are unlikely to follow the distribution. These tests have been applied in other submarine landslide studies (Casas et al., 2016; Geist & ten Brink, 2019).

3.4. Estimates of Peak Horizontal Accelerations During Earthquakes

Earthquake-induced ground motions have been widely suggested to trigger landslides (Fine et al., 2005; Gràcia et al., 2003; Heezen & Ewing, 1952; Tappin et al., 2001). Earthquakes with $Ms > 6.5$, which can create a local peak horizontal acceleration (PHA) >0.5 g, occur every 70 years on average in the Azores (Nunes & Ribeiro, 2001; Nunes et al., 2001). To compare with the landslide data, we estimated PHA as follows. Moment magnitudes *Mw* were derived from all 1964–2019 body-wave magnitudes (m_b), duration magnitude (M_d), and local magnitude (M_L) of the ISC catalog using the following relations (Das et al., 2011 for m_b, Kadirioğlu & Kartal, 2016 for M_d, and Castello et al., 2007 for M_L):

$$M_w = \exp\left(0.719 + 0.212 m_b\right) - 0.737 \tag{1}$$

$$M_w = 0.7947 M_d + 1.342 \tag{2}$$

$$M_w = 0.79 M_L + 1.2 \tag{3}$$

Based on an empirical study of ground motion recordings in western North America, Boore et al. (1997) suggested the following dependence of PHA (Y in fraction of g) on *Mw* and closest horizontal distance from source (r_{jb} in km).

$$\ln Y = b_1 + b_2\left(Mw - 6\right) + b_3\left(Mw - 6\right)^2 + b_5 \ln r + b_V \ln\left(V_S / V_A\right) \tag{4}$$

$$r = \left(r_{jb}^2 + h^2\right)^{1/2}$$

V_S is average shear-wave velocity of the upper 30 m in m/s used to represent local site conditions. Parameters V_A (m/s) and h (m) are fictitious values found by the regression analysis. Coefficients b_1, b_2, b_3, b_5, h, b_V, and V_A are determined by nonlinear regression (Joyner & Boore, 1994), which in this study were derived from Boore et al. (1997, their Table 8) corresponding with period 0.75 s as suggested by ten Brink et al. (2009). The 200 m/s value used here for *Vs* is a representative average for 0–30 m depth in marine sediments from data compiled by Hamilton (1976). Equation 4 was derived from larger magnitude earthquakes than we study here and represents effects of attenuation and scattering over continental crust, so the derived PHA could be biased, though we use it here as it is based on a large amount of strong-motion data and lack of suitable alternatives.

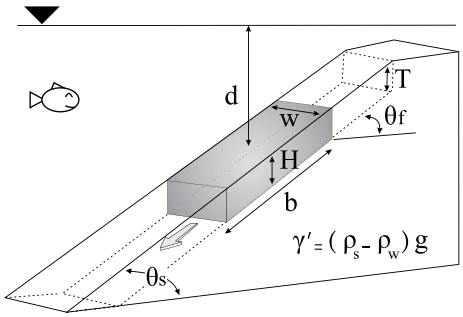

Figure 4. Shallow slope failure parameters used in the static limit-equilibrium calculation and estimates of tsunami height at source.

3.5. Sediment Cohesion Estimates

Geotechnical data are not available to assess the stability of these slope sediments. However, remarkably steep deposits in headwalls and, in places, chutes of landslides (Figures 1b–1e) around the volcanic islands imply that the slope sediments are cohesive and that in turn has implications for how we interpret them. In contrast, if the slopes were instead purely incohesive sediment, they would be expected to have gradients no greater than the angle of repose of ~30°. We estimated cohesion by inverting the conventional equations used in static limit-equilibrium analysis using the seabed gradients found. Such analysis is still widely applied due to its simplicity and ease of usage but tends to be conservative (Jibson, 2011), implying that cohesion estimates based on it will be minima. According to that analysis, failure occurs when the factor of safety (FS) (the ratio of resisting to driving stresses on the potential failure surface) is lower than 1. We use the simplified equations for failure on a surface parallel to the dipping seabed (Figure 4), assuming the structure extends infinitely. FS is then simply given by:

$$\mathrm{FS} = \left[c/\left(\gamma' H \cos\theta_f \sin\theta_f\right)\right] + \left(\tan\Phi/\tan\theta_f\right) \tag{5}$$

$$\gamma' = \left(\rho_s - \rho_w\right) g$$

where c = sediment cohesion, H = average thickness of failure, γ' = unit weight of submarine deposit in water, ρ_s = sediment wet bulk density and ρ_w = water density, g = gravitational acceleration, θ_f = the angle of failure, and Φ = sediment friction angle. Using parameters given later, we estimated c as the value satisfying FS = 1. As earthquake shaking was not considered but some of these steep sediments may have survived such shaking, this analysis provides a minimum value for c.

3.6. Estimates of Tsunami Height

Coastal runup heights of tsunamis are difficult to reconstruct without sophisticated numerical modeling. There is also the uncertainty over whether the valleys were created by single or multiple landslides (Hunt et al., 2011, 2013). Nevertheless, Watts et al. (2003) derived analytical expressions for the initial waves above the landslides that are potentially useful for applying to the Azorean valleys likely produced by single events. Those expressions were derived from laboratory experiments simulating landslides that are large along-slope compared with the tsunami wavelength. McAdoo and Watts (2004) updated the expressions to allow for landslides that are narrower along-slope than the tsunami wavelength. In their model, the sliding body was idealized as elliptical with specific gravity 1.85. With further corrections by De Lange and Moon (2004), this wave amplitude at source for translational slides is:

$$A = 0.224T\left[w/\left(w+\lambda\right)\right]\left[\left(\sin\theta\right)^{1.29} - 0.75\left(\sin\theta\right)^{2.29} + 0.170\left(\sin\theta\right)^{3.29}\right]\left(b/d\right)^{1.25} \tag{6}$$

$$\lambda = 3.87\left(bd/\sin\theta\right)^{1/2}$$

where (Figure 4) T = head scarp height, w = along-slope landslide width, λ = tsunami wavelength, θ = average slope angle, b = initial length of the slide measured downslope, and d = depth of landslide initial center of mass. Sediment density has not been measured here. If, based on the offshore cores, our suspicion that the sediment comprises detrital particles is correct, a wet bulk density of ~2.0 g/cm^3 is appropriate (Hamilton & Bachman, 1982) so the specific gravity of 1.85 should not be far in error. Spreading during wave propagation toward the coasts can reduce wave amplitudes, whereas shoaling typically increases wave amplitudes. Local bathymetry can refract waves, leading to either convergence or divergence. Depending on direction, the incoming waves can also interfere with wave fronts emanating from the landslide deposit area (Geist et al., 2009). Local wave impacts are therefore likely to vary greatly around coasts and differ from these values of A. Nevertheless, Casalbore et al. (2011) found that tsunami runup heights in the Tyrrhenian Sea roughly compared with those predicted by Equation 6. Here, the estimated values of A were used mainly to provide a rough sense of relative scale, in a similar way to how earthquake magnitudes are used to assess relative size.

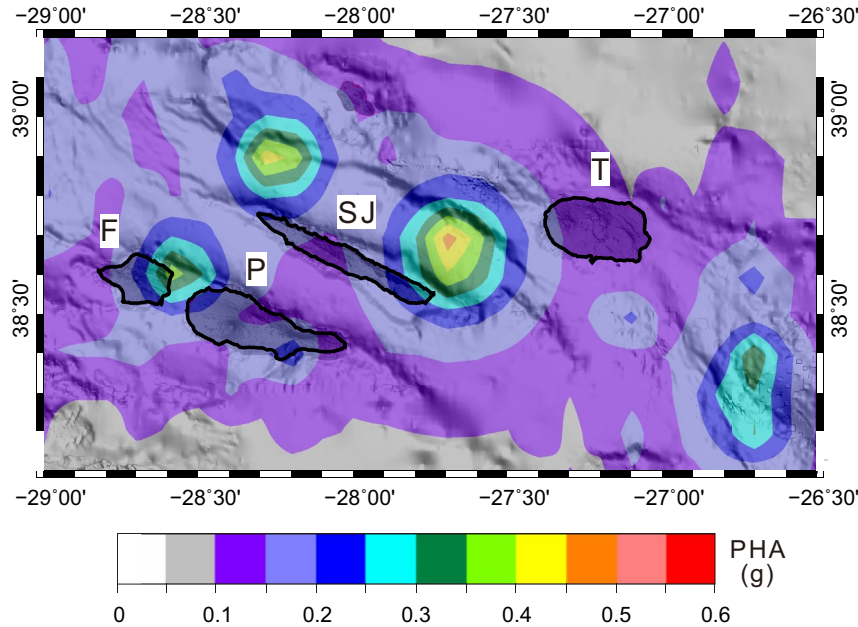

Figure 5. Peak horizontal accelerations (PHA) derived from the International Seismological Centre catalog for 1964–2019 earthquakes. F, P, SJ, and T are Faial, Pico, São Jorge, and Terceira, respectively.

4. Results

4.1. Seismic Ground Shaking

The map of PHA (Figure 5) calculated from the ISC data (Figure 2) suggests that the submarine slopes of the four islands studied here have all experienced >0.05 *g* and locally >0.4 *g* since 1964. Three areas of high acceleration occur around the slopes of Faial and São Jorge associated with the largest earthquakes in the ISC catalog. However, if our suspicion is correct that the landslides have formed over the Holocene, all of these slopes may have experienced as much as 0.5 *g* PHA over that timescale for at least two reasons. First, the historical (1522–1964) record includes 10 large events (Figure 2), many of which occurred on Terceira where seismicity since 1964 has been modest (Figure 2). This suggests a discrepancy with the instrumental data. Although magnitudes of such old events are difficult to estimate accurately, they are likely to have been $M > 6.5$ based on magnitude assessments of historical records elsewhere (Nunes & Ribeiro, 2001; Nunes et al., 2001). Second, active faults are widespread amongst the islands. Madeira et al. (2015) estimated that >20-km-long faults on the islands could produce events of $M = 6.5$ if they ruptured along their whole lengths. However, mapping the full extents of active faults is difficult on land, where they can be masked by subsequent deposits (Hipólito et al., 2014). Identifying active faults between the islands and continuations of faults from land underwater is another challenge. Deep-tow sonar images (Mitchell et al., 2018) show many fault escarpments that lack erosional features seen in older inactive faults (Tucholke et al., 1997), and the FAIVI data also show many "fresh" submarine fault scarps around Terceira (Casalbore et al., 2015; Chiocci et al., 2013; Quartau et al., 2014). We thus suspect that the submarine areas host active faults, as also implied by the broad distribution of seismicity. Many of these faults have greater lengths than those mapped on land by Madeira et al. (2015) so they likely generate earthquakes larger than the $M = 6.5$ that Madeira et al. (2015) suggested as a maximum. Consequently, the pattern of seismic accelerations over the long-term remains uncertain.

4.2. Submarine Landslide Inventory and Volume-Frequency Distribution

We mapped 1,227 slope valleys in total. The counts of the different classes and types are shown in Figures 6a and 6b. Volumes range from 10^2 to 10^8 m^3 with sample mean 7.9×10^5 m^3. The volume distribution for all valleys (Figure 6c) has a logarithmic bell shape. The volume distributions for individual islands (Figure 6d) differ from each other. The modes for Pico and Faial (10^4–10^5 m^3) are smaller than those for São Jorge and

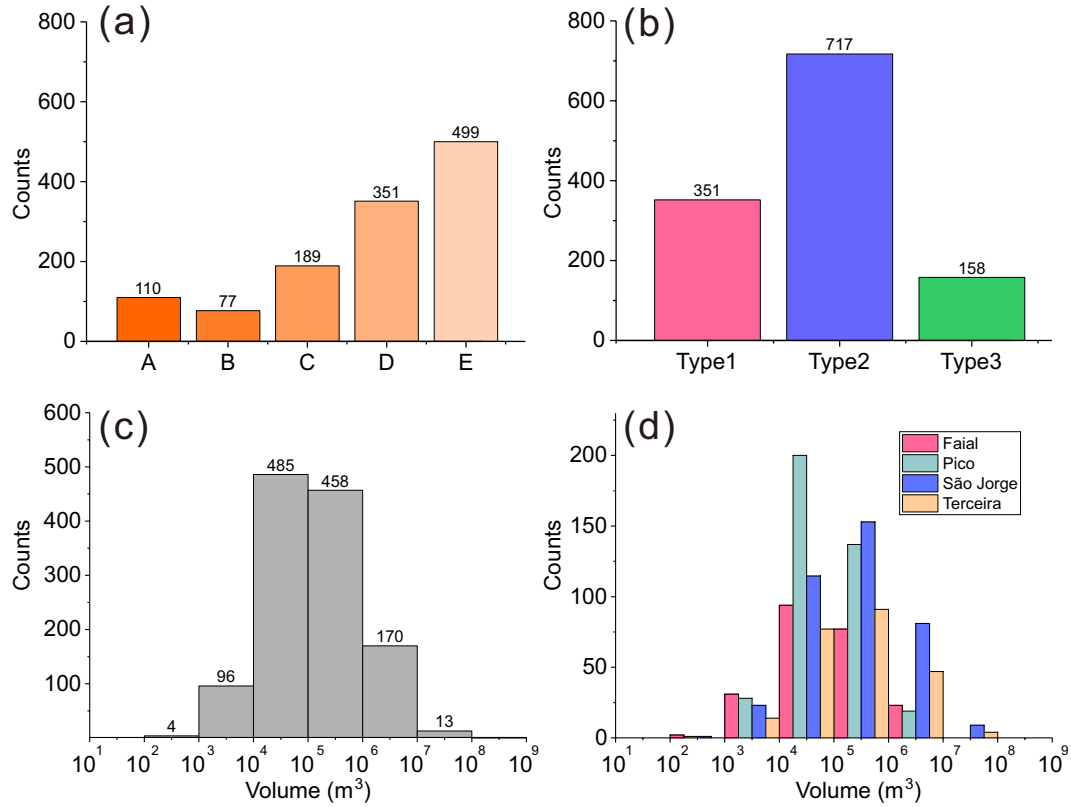

Figure 6. Histograms of slope valleys. (a) Counts by class. (b) Counts by type. Colors in (a) and (b) are as Figure 3 (right panels). (c) Counts of volumes of all mapped slope valleys. (d) As (c) for individual islands. Values above bars in (a, c, d) are counts in each interval.

Terceira (10^5–10^6 m^3), but the distributions all have similar bell shapes. Figure 6d also reveals that São Jorge and Terceira have higher percentages (20%–25%) of the larger valleys ($V > 10^6$ m^3) than Faial and Pico islands (5%–10%). The largest 10 valleys (all types) all occur around São Jorge and Terceira. São Jorge and Terceira also have the largest valley cumulative area and volume (Figures 7a and 7c), an observation that persists when the data are normalized for slope area (Figures 7b and 7d).

The relationship between area (A_l) and volume (V) for valleys most likely to be single landslide scars (type 2 and classes A–C) is shown in Figure 8. Regressing the logarithmic variables suggests $V = 0.234 A_l^{1.3365}$ ($R^2 = 0.924$). Mean thicknesses were also obtained by dividing individual landslide scar volume by area (also for type 2 and classes A–C valleys). The mean thicknesses are 9.2 ± 0.5, 7.3 ± 0.5, 12.6 ± 0.8, and 10.6 ± 1.3 m for Faial, Pico, São Jorge, and Terceira, respectively (uncertainties of means are 1σ). CCDFs of area and volume were also generated from these valleys (type 2 and classes A–C) as shown in Figure 9. Both CCDFs follow log-normal distributions ($p = 0.98$ and 1.0).

4.3. Assessment of Cohesions of Steep Deposits

Steep gradients in some headwalls and sidewalls exceed 60° locally and generally reach 30°–40° (Figures 1b and 1c). Using these slope gradient values for the failure gradient angle, we inverted Equation 5 for cohesion c. For H, we used the average thickness (10.6 m) of the scars associated with single landslides (type 2 and classes A–C) found by dividing their volumes by their areas. A bulk density of 1.0 g/cm^3 was used for (ρ_s–ρ_w) representing sand in water (Hamilton & Bachman, 1982; Hamilton et al., 1956). We used 25°–40° for internal friction angle Φ typical of volcaniclastic sands and calcareous ooze (Boldini et al., 2009; Lee et al., 1994). Repeating the calculation for gradients of 30°–60°, we estimated c between 9 and 33 kPa (Figure 10). However, these c-values are minima because the infinite-slope calculation is conservative. Furthermore, if some of these steep sediment deposits have survived shaking by earthquakes, such accelerations have not been

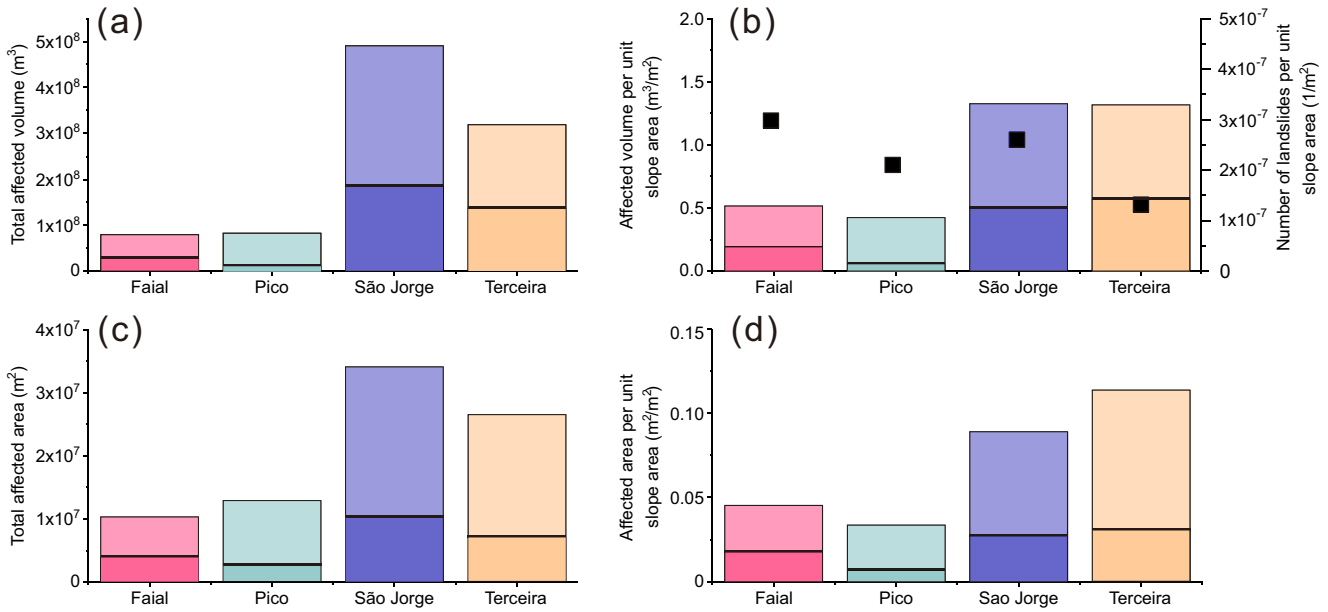

Figure 7. Summaries of total areas and volumes of slope valleys of each island (all types and classes; bold colors represent the volumes of the type 2, classes A–C valleys only). (a) Total volume of valleys. (b) As (a) normalized to submarine slope area of each island. Solid squares show the abundances of the type 2, classes A–C valleys (scale to right). (c) Total area of valleys. (d) As (c) normalized to submarine slope area of each island.

taken account of by only the gravitational loading used in Equation 5, also ensuring that these c-values are minima.

The upper-slope sediments lie in water that is saturated with respect to aragonite and calcite (Wisshak et al., 2010, 2015), so cementation may be involved in stabilizing the sediments. Carbonates are precipitated from seawater on the edges of clasts (Gabitov et al., 2019), binding the sediments (e.g., Tucker et al., 2020). These cohesion values (Figure 10) noticeably overlap with laboratory results of Nafisi et al. (2020), who formed calcium carbonate cements in sand by microbial precipitation and tested the results under 10–100 kPa effective stresses. They showed that cohesion was 9–12 kPa after moderate cementation (1–4 wt% $CaCO_3$) and 56–65 kPa after high cementation (4–10 wt% $CaCO_3$). Our 9–33 kPa estimates of sediment cohesion therefore correspond with moderate to high cementation.

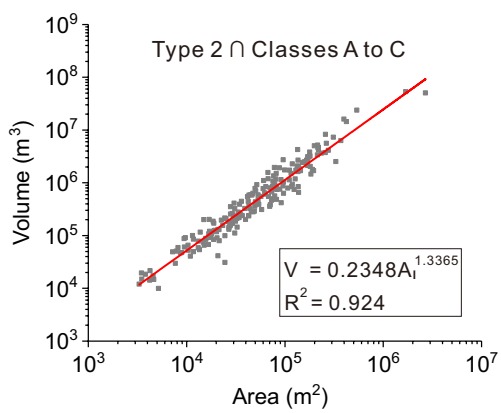

Figure 8. Empirical relationship between area (A_l) and volume (V) for the central Azores valleys of type 2 and classes A–C. A least squares regression of the logarithmic variables suggests the relationship shown (red line).

These cohesion values are also compatible with test results on some volcaniclastic deposits (e.g., lava-breccia ~30 kPa) found in volcanic islands as here but lower than the ~600 kPa of pyroclastic deposits (Di Traglia et al., 2018). Volcaniclastic deposits lying at up to 40° were also found off the Sciara del Fuoco slope of Stromboli (Casalbore et al., 2020). Some of these cohesions could therefore be compatible locally with lava deltas (Mitchell et al., 2008) underlying parts of these slopes. The cohesions we estimated are logically smaller than found in intact rocks (c > 25,000 kPa; Bieniawski, 1975; Marinos & Hoek, 2000).

4.4. Assessment of Tsunami Wave Heights at Source

Tsunami heights A immediately above landslides were derived for 83 single-failure landslides (type 2) with $V > 10^6$ m^3 using Equation 6 (detailed morphometric data in Supporting Information S1). The CCDF of wave height in Figure 11a also follows a log-normal model ($p = 0.43$). We define an initial wave height at source >1 m as potentially hazardous as such a wave could be amplified to several meters when inundating coasts

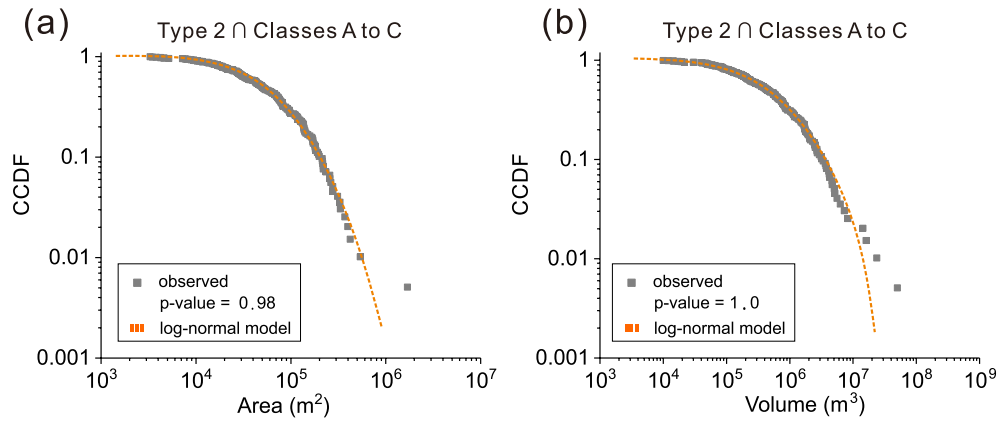

Figure 9. Complementary cumulative distribution functions (CCDFs) of (a) area and (b) volume for valleys most likely to be landslide scars (type 2 and classes A–C). Orange dashed lines are log-normal models. Note that axes are logarithmic.

(e.g., Tinti et al., 2005). At least 18 landslides were found capable of generating tsunamis with $A > 1.0$ m, and one with $A > 7$ m (Figure 11). These landslides were located around São Jorge, Terceira and Faial Islands.

Sophisticated modeling of landslide-triggered tsunami wave propagation is beyond the scope of this paper. Coastal topography, refraction and wave steepening with shallowing water all affect final runup height (tides are a secondary consideration here as they are only ~1 m [Cruz & Silva, 2001]). However, a first-order estimate of tsunami height at the coast can be made using Green's law (e.g., Federici et al., 2006), which predicts runup heights relative to source heights. In our study area, the shoaling factor to 1 m water depth is between 3 and 5, suggesting that there is an underappreciated risk of tsunamis around volcanic islands such as the Azores.

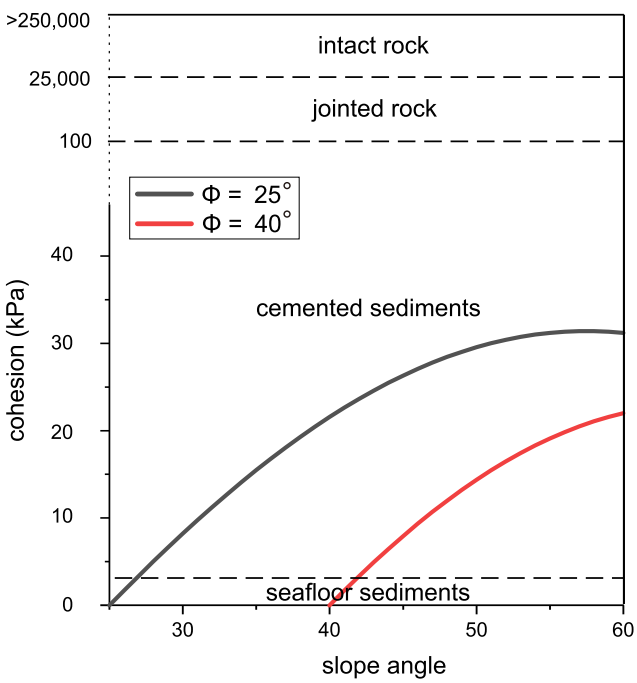

Figure 10. Estimates of sediment cohesion with varied slope angles from the pseudo-static analysis with no seismic accelerations. Dashed lines represent typical cohesion values for the materials shown.

5. Discussion

5.1. Assessing Varied Submarine Landslide Features in the Central Azores

The above analysis has revealed lower cumulative volumes and areas of slope valleys around Faial and Pico islands than around São Jorge and Terceira islands (Figure 7). The density of landslides around São Jorge is comparable with those of Faial and Pico, so landslides around São Jorge are generally larger than those around the other two islands. Accounting for the low density but high affected slope volume of landslides in Terceira Island, the landslides there are large as well. As might be expected from their different average volumes, therefore, landslides are modestly thicker on average around São Jorge than around Faial and Pico. We explore these contrasts in this section.

5.1.1. Earthquake Triggering

ten Brink et al. (2016) suggested that slopes become more stable with decreasing sedimentation rate and increasing frequency of earthquakes. Such increased sediment shear strength arises due to seismic shaking, causing shear-induced compaction (e.g., Sawyer & DeVore, 2015; ten Brink et al., 2016) or sediment internal structure changes (Wu et al., 2021). This may help to explain the comparatively high 9–33 kPa estimated cohesion of these Azorean sediments besides carbonate cementation and prompts us to ask if earthquakes may explain other aspects of the landslides data also. To represent the regional occurrences of landslides, we prefer the

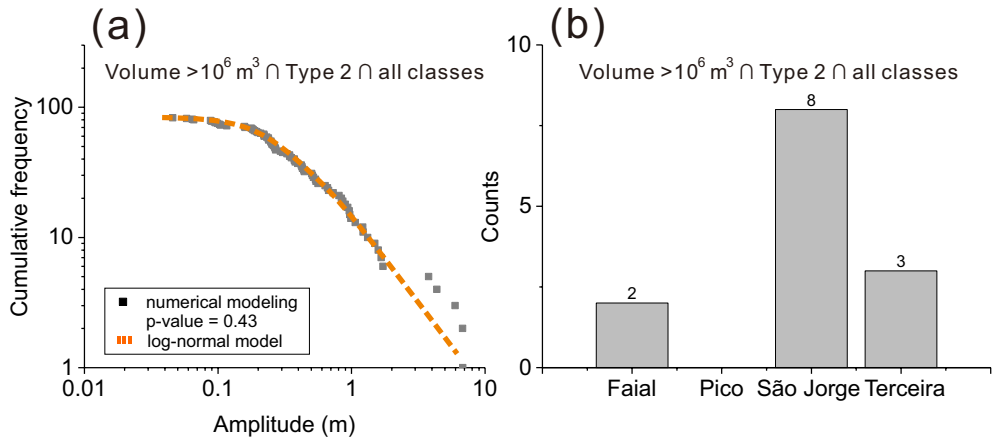

Figure 11. Cumulative frequency of tsunami amplitudes (A) at source predicted using Equation 7 from landslide scars (volumes $>10^6$ m^3, type 2, all classes), depths and other characteristics. (b) Occurrences of potentially hazardous tsunamis ($A > 1$ m) for individual islands.

cumulative volumes or areas of all slope valleys (Figure 7) as they form the largest database, although the restricted groups (type 2 and classes A–C) also show a similar tendency for volumes and areas of valleys around São Jorge and Terceira to be larger than those around Faial and Pico islands.

The pattern of extreme shaking in Figure 5 is dominated by the three largest earthquakes occurring since 1964, with two near São Jorge and one in northeast Faial. The pattern does not correspond with the landslide volume and area differences between the islands. However, the lack of correspondence could arise if the ISC catalog is unrepresentative of the long period over which these submarine landslides likely developed (>ky). For example, patterns of seismicity can change location over decades due to changes in stress after the largest events (Stein, 1999). The historical record of earthquakes is also subject to uncertainties. The wide distribution of active faults (Figure 2) implies that there is a potential for large earthquakes that is more widespread than suggested by the simplistic reading of either instrumental or historical records.

Sediments accumulating on the upper island slopes originate from various sources; from coastal and subaerial erosion, biological production and volcanic eruptions. Their fluxes are hard to quantify and most likely vary around the islands. However, a simple explanation for the larger landslides around São Jorge and Terceira compared with Faial and Pico could involve a larger time interval between destructive earthquakes, leaving more time for deposits to accumulate. This in turn implies that there could be a higher frequency of larger earthquakes around Faial and Pico islands and thus a greater longer-term threat of earthquakes there. This is an important inference concerning the seismic hazards of the Azores islands. We however temper this inference by assessing other factors below that may have also affected the landslide volumes and areas.

5.1.2. Varied Lava Flow Types

Lava flows on east Pico island are mainly 'a'a whereas those of west Pico are more mixed pahoehoe and 'a'a types (Figure 1). Pahoehoe flows typically form stacks of thin sheets whereas 'a'a lava flows are commonly thicker (Macdonald, 1953). Although 'a'a flows can have friable clinkers above and below them, their interiors are commonly more massive and less porous or fractured (Macdonald, 1953). During sea-level low-stands, lava flows would have more easily reached the outer shelves, supplying the uppermost slopes directly. Although we anticipate there being mainly sediments underlying the uppermost slopes because turbidites in offshore cores contain mainly silt-sand grade volcaniclastic and bioclastic particles (Chang et al., 2021), different landslide statistics may occur if there were widespread lava underlying the upper slopes because of differences in geotechnical properties between the two lava flow types.

However, landslide volumes (Figure 12) differ only slightly between west and east Pico. We suggest that, even if lavas are common, volcaniclastic deposits of 'a'a and pahoehoe are probably similarly susceptible to failure, rapidly disaggregating on the steep upper submarine slopes (cf. Sansone & Smith, 2006). Furthermore, varied effusion rates of lava flows and the pre-eruption seafloor morphology can also lead to uneven

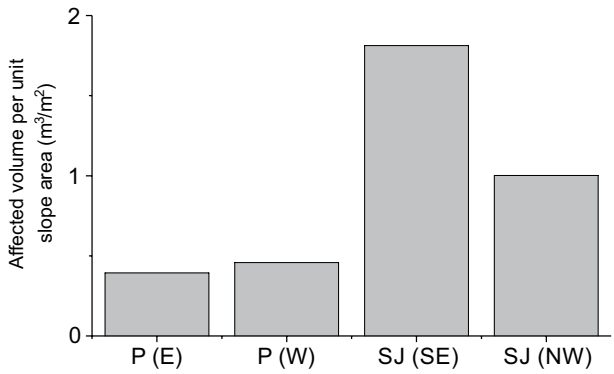

Figure 12. Cumulative volumes of slope valley per unit slope area for subdivisions of Pico and São Jorge islands (all valley classes and types).

loading of slopes by lava flows, which ultimately affect slope stability (Bosman et al., 2014; Casalbore et al., 2021), so factors other than merely flow type likely affect landslide occurrences.

5.1.3. Volcanic Ages of Adjacent Land and Shelf Widths

The ages of the volcanic sequences comprising each island might be expected to influence landsliding if more recent volcanic building led to steeper slopes of friable material that were, susceptible to failure. On the other hand, broad shelves typical of older volcanic islands (Menard, 1986) may host thick sediments and those sediments may be exported to the island submarine slopes by wave erosion and/or mass wasting (e.g., Dengler et al., 1984; Fornari et al., 1979). Based on high-resolution bathymetry data, Quartau et al. (2010, 2014, 2015) confirmed that most of the older volcanoes in the Azores have wider shelves than younger edifices, though shelf width can be affected by vertical tectonic motions, varied wave climate and other factors as well (Ramalho et al., 2013). As sediments are continually produced by biogenic production as well as subaerial erosion and wave abrasion of sea cliffs, we might expect the upper slopes of islands with wide shelves to be capable of accumulating thicker sediment deposits during sea-level high-stands. For instance, the easterly older shelf of São Jorge has a broad sedimented terrain where seismic data reveal an extreme ~250 ms of layered sediment (Marques et al., 2018). However, shelf width is likely not the sole pre-conditioner for slope failures. For instance, Santa Maria, which is the oldest island and has the widest shelf of the Azores, has deposits on its shelf of only a few m thick (Ricchi et al., 2020). This is partly because it is a low relief, semi-arid island and hence contributes little sediment from stream erosion. In addition, wide shelves can attenuate waves crossing them, protecting cliffs from erosion (Ricchi et al., 2020).

Although São Jorge has a higher cumulative volume of slope valleys than either Faial or Pico islands, there are also differences between the volcanically old and young parts of São Jorge. The slope valleys in old southeast São Jorge have nearly twice the volume per unit slope area than those in the young northwest part of the island (Figure 12). This favors an explanation involving export of shelf sediment from the broad shelf in southeast São Jorge, leading to thick slope deposits susceptible to failure. Sediment production rates are difficult to anticipate, given that the sediments originate from varied sources such as biogenic particles created on the shelves, subaerial and coastal erosion, and pyroclastic fallout from eruptions (Quartau et al., 2012), though collecting sediment cores and other data around the islands could in principle help resolve this in the future. Nevertheless, the thick sediment imaged seismically beneath the shelf of São Jorge (Marques et al., 2018) suggests this could indeed partly explain its high cumulative volume of slope valleys. Despite this effect, the cumulative volumes of landslide valleys of west São Jorge (~1 m^3/m^2), where the island is volcanically young and the shelf is narrow, is still larger than the volumes for Faial and Pico, which are both <0.5 m^3/m^2, so the difference between the islands still needs an explanation, such as the difference in long-term seismicity.

5.2. Comparing the Azores Landslide Area-Volume Relationship With Those of Other Settings

The relationship between volume (V) and area (A_l) is generally written as $V = \alpha A_l^{\beta}$ where α and β are constant parameters for each data set. Landslides that are perfectly self-similar or show no systematic variation in ratio between the vertical and horizontal dimensions should uniformly have $\beta = 1.5$ (Guzzetti et al., 2009; Klar et al., 2011). With accurate landslide dimensional measurements, Guzzetti et al. (2009) reported $\beta = 1.449$ for subaerial landslides in central Italy, which is close to $\beta = 1.5$.

Table 1 shows α and β values for six studies of data from different submarine geological environments for comparison with the Azores results. ten Brink et al. (2006) suggested that diverse β values could result from different failure processes and thicknesses of failed material. For instance, clay-rich debris lobes in the Storegga slide of Haflidason et al. (2005) have β close to 1 $\left(V = 0.0267 A_l^{1.032}\right)$, a result of a nearly constant thickness of the sliding layer regardless of slide area. Other regions with β close to 1 (Chaytor et al., 2009; Hu et al., 2009) are located in open continental slopes where gradients are gentle and sediments have been

Table 1
Synthesis of Volume-Area Relationships

	Number	α	β	References
Central Azores	197	0.2348	1.337	This study
Southern Tyrrhenian Sea	428	0.0009	1.369	Casas et al. (2016)
US Atlantic margin	106	0.0163	1.099	Chaytor et al. (2009)
East China Sea	102	0.0260	1.020	Hu et al. (2009)
Puerto Rico	160	0.2630	1.292	ten Brink et al. (2006)
Mediterranean Sea	696	0.0050	1.251	Urgeles and Camerlenghi (2013)

homogeneously deposited, though likely having layered physical properties. Failure along seabed-parallel layers tends to form tabular landslides. A Mediterranean result (Urgeles & Camerlenghi, 2013) has intermediate $\beta = 1.251$. The Mediterranean slopes have varied geological structure and sedimentary inputs, leading to diverse landslides types and thickness.

The Azores data have intermediate $\beta = 1.337$, though closer to a size-invariant ratio ($\beta = 1.5$). Landslides have $\beta < 1.5$, perhaps because of later infilling of valleys by sediments or resistance to deep failure (e.g., because of increasing sediment compaction or harder volcanic rocks at depth).

5.3. Comparing Cumulative Volume Distributions With Those of Other Areas

Figure 13 shows CCDFs of landslide volume from seven different submarine settings. CCDFs are used to assess the maximum size in a region and investigate the relative occurrences of features of differing size, though are affected by completeness and other factors. Substantial sediments can accumulate on open passive continental margins as the slopes are broad and homogenous, with only occasional earthquakes. However, once landslides occur, movements can transport sediment far from their origins so landslides can be large, reflected in their CCDFs (ten Brink et al., 2006). Though landslides in tectonically active areas are usually small (Urgeles & Camerlenghi, 2013), some giant submarine landslides still can be produced there (e.g., large slumps in Hawaii; Masson et al., 2002).

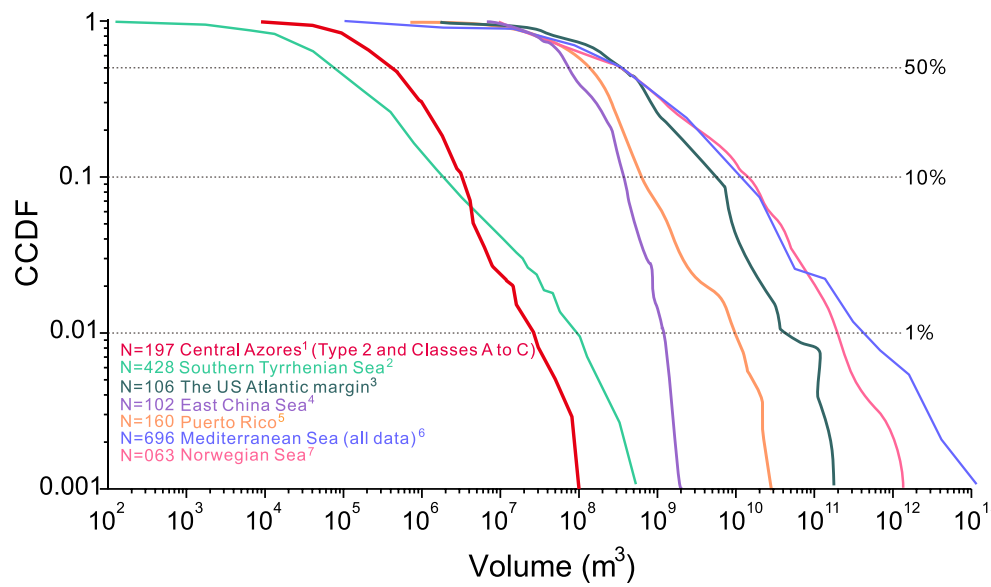

Figure 13. Complementary cumulative distribution functions (CCDFs) of landslide volumes ([1] This study, central Azores; [2] Casas et al., 2016, southern Tyrrhenian Sea; [3] Chaytor et al., 2009, US Atlantic margin; [4] Hu et al., 2009, East China Sea; [5] ten Brink et al., 2006, Puerto Rico; [6] Urgeles & Camerlenghi, 2013, Mediterranean Sea; [7] Haflidason et al., 2005, middle Norwegian Sea).

Small landslides (<10^5 m^3) tend to be identified more readily in higher-resolution data sets. Hence, at least 10 times more landslides were identified in bathymetry grids with 20-m cell sizes than in those with 100-m cell sizes (Figure 13). Comparing data sets of similar grid cell sizes, some differences occur that could be explained by differing sediment physical properties. For instance, the smallest mapped scars in the Azores have volumes 5 times larger than the smallest scars in the southern Tyrrhenian Sea, despite comparable grid cell sizes (<20 m). One possible explanation could be different sediment cohesions. Limit-equilibrium slope stability modeling has suggested that incohesive sediments tend to form shallow, elongate landslides with no lower size limit, whereas cohesive sediments tend to develop landslides with a minimum size (Frattini & Crosta, 2013). The 9–33 kPa or larger cohesion of the Azores sediments may explain the larger minimum volumes there compared with those of the Tyrrhenian Sea. However, the variance of geological setting needs to be considered as well, as most of the small landslide scars in the Tyrrhenian Sea were found at the heads or flanks of submarine canyons. Confined spaces there may also have limited landslide development (Casas et al., 2016).

5.4. Lessons for Assessing Geohazards of Volcanic Islands

We have suggested that differences in the cumulative volumes and areas of submarine landslides may imply differences in long-term seismicity. Such differences could potentially help to overcome the inadequacy of the instrumental seismic record (Scholz, 2002). Hence, submarine landslide mapping can help in assessing earthquake hazards as well as tsunami hazards. This analysis could easily be repeated around other volcanic islands with suitable bathymetric data, although effort is still needed to assess the other possible causes of varied landslide properties identified above, for example, fluxes of sediment from erosion and biogenic production.

Geotechnical data would help evaluating slope responses to earthquakes. Obtaining samples for such tests by vibrocoring would be challenging on the steep (30°) slopes of islands, but more indirect assessments of sediment rigidity may be possible, for example, velocities from shallow seismic refraction.

More efforts could be put into assessing landslide frequency. Long-term records can be obtained by dating landslide-origin turbidites (e.g., Hunt et al., 2013). Short-term records could be obtained by repeating multibeam sonar surveys (e.g., Casalbore et al., 2012, 2020; Kelner et al., 2016; Soule et al., 2021), with timings of events obtained from tide gauge records and acoustic recordings (Caplan-Auerback et al., 2001) to help identify possible formative events such as earthquakes.

6. Conclusions

We have mapped 1,227 submarine slope valleys in the central Azores volcanic islands. To overcome difficulties of interpretation arising from the rugged morphology of the upper submarine slopes, valleys were first categorized based on the levels of recognition as landslides and whether they appear to have formed by single, multiple or retrogressive failures events.

Considering slope valleys of all types and classes, São Jorge and Terceira islands have greater valley volumes and areas per unit slope area, compared with Faial and Pico. We highlight this observation as suggesting that Faial and Pico potentially have greater earthquake hazard. In this interpretation, frequent earthquakes prevent the build-up of unstable sediment deposits on slopes, leading to mostly smaller landslides around Faial and Pico. This suggestion is tempered by an observed greater valley volume in easterly São Jorge where thick sediments are also observed on its shelf. Such sediments are likely exported to slopes during sea-level lowstands, which suggests that greater sediment accumulation has also affected landslide volumes there. Nevertheless, westerly São Jorge has a narrower shelf and its valley volume is still greater than Faial and Pico islands. Thus, differences in factors other than sediment input such as seismicity are still needed to explain the contrast in slope valleys statistics.

Cumulative area and volume distributions for valleys most likely to be single landslides fit log-normal probability density functions, as found elsewhere. Based on an analytical formula, at least 13 of the valleys most likely to have been produced by single landslides would have generated tsunamis with heights >1 m at

source. One may have produced a wave of ~7 m. Those heights also follow a log-normal probability density function.

Static slope stability analyses suggest that some steep slopes have cohesive strengths of at least 9–33 kPa, much larger than 0.08–2 kPa expected of typical superficial incohesive seafloor sediment. This could be explained by moderate to high carbonate cementation, by earthquakes shaking and/or perhaps by the presence of coherent lava or talus.

Overall the study suggests that mapping submarine landslides around volcanic islands in general could also be useful for investigating seismic and tsunami hazards that are not well characterized by other methods, as well as uncovering other aspects of their submarine slope sediments.

Data Availability Statement

The 2003 multibeam data are available at 100 m grid resolution from the Marine Geoscience Data Portal (http://www.marine-geo.org/index.php). The multibeam data for Terceira are not publicly available due to the sensitive nature of the area and environmental sustainability concerns, but can be made available to researchers with appropriate credentials. Background bathymetric data are from the GeoMapApp (GMRT; www.geomapapp.org, Ryan et al., 2009). The seismic catalog is from International Seismological Centre (2019) (https://doi.org/10.31905/EJ3B5LV6; Di Giacomo et al., 2014).

Acknowledgments
Yu-Chun Chang thanks the editor Peter van der Beek and reviewers Daniel Casalbore and Uri ten Brink for their constructive comments, which led to significant improvements of this manuscript. He also thanks the Taiwanese government for providing his PhD scholarship and the International Association of Sedimentologists for a travel grant to the annual British Sedimentological Research Group meeting, where some of these ideas were explored. The European Communities 7th Framework Programme under EUROFLEETS funded the bathymetric data collection around Terceira used in this study. Iasmina Cristina Popa is thanked for a preliminary attempt at the peak ground horizontal analysis. Thor Hansteen, Christoph Beier, Adriano Pimentel, Ting-Wei Wu, Sung-Ping Chang, and Zhongwei Zhao are thanked for informative discussions. Figures were prepared with the GMT software system (Wessel & Smith, 1991).

References

Alberico, I., Budillon, F., Casalbore, D., Di Fiore, V., & Iavarone, R. (2018). A critical review of potential tsunamigenic sources as first step towards the tsunami hazard assessment for the Napoli Gulf (Southern Italy) highly populated area. *Natural Hazards*, *92*, 43–76. https://doi.org/10.1007/s11069-018-3191-5

Andrade, C., Borges, P., & Freitas, M. C. (2006). Historical tsunami in the Azores archipelago (Portugal). *Journal of Volcanology and Geothermal Research*, *156*, 172–185. https://doi.org/10.1016/j.jvolgeores.2006.03.014

Barrett, R., Lebas, E., Ramalho, R., Klaucke, I., Kutterolf, S., Klügel, A., et al. (2019). Revisiting the tsunamigenic volcanic flank-collapse of Fogo Island in the Cape Verdes, offshore West Africa. *Geological Society, London, Special Publications*, *500*, 26. https://doi.org/10.1144/SP500-2019-187

Bieniawski, Z. (1975). *Case studies: Prediction of rock mass behaviour by the geomechanics classification*. Second Australia-New Zealand Conference on Geomechanics (p. 36). Institution of Engineers.

Boldini, D., Wang, F., Sassa, K., & Tommasi, P. (2009). Application of large-scale ring shear tests to the analysis of tsunamigenic landslides at the Stromboli volcano, Italy. *Landslides*, *6*, 231–240. https://doi.org/10.1007/s10346-009-0155-6

Boore, D. M., Joyner, W. B., & Fumal, T. E. (1997). Equations for estimating horizontal response spectra and peak acceleration from western North American earthquakes: A summary of recent work. *Seismological Research Letters*, *68*, 128–153. https://doi.org/10.1785/gssrl.68.1.128

Bosman, A., Casalbore, D., Romagnoli, C., & Chiocci, F. L. (2014). Formation of an 'a'a lava delta: Insights from time-lapse multibeam bathymetry and direct observations during the Stromboli 2007 eruption. *Bulletin of Volcanology*, *76*. https://doi.org/10.1007/s00445-014-0838-2

Calvert, A. T., Moore, R. B., McGeehin, J. P., & Rodrigues da Silva, A. M. (2006). Volcanic history and $^{40}Ar/^{39}Ar$ and ^{14}C geochronology of Terceira Island, Azores, Portugal. *Journal of Volcanology and Geothermal Research*, *156*, 103–115. https://doi.org/10.1016/j.jvolgeores.2006.03.016

Caplan-Auerback, J., Fox, C. G., & Duennebier, F. K. (2001). Hydroacoustic detection of submarine landslides on Kilauea volcano. *Geophysical Research Letters*, *28*, 1811–1813. https://doi.org/10.1029/2000GL012545

Carvalho, A., Sousa, M., Oliveira, C., Campos-Costa, A., Nunes, J., & Forjaz, V. (2001). Seismic hazard for the central group of the Azores islands. *Bollettino di Geofisica Teorica ed Applicata*, *42*, 89–105.

Casalbore, D., Bosman, A., & Chiocci, F. L. (2012). *Study of recent small-scale landslides in geologically active marine areas through repeated multibeam surveys: Examples from the southern Italy* (pp. 573–582). Springer Netherlands. https://doi.org/10.1007/978-94-007-2162-3_51

Casalbore, D., Di Traglia, F., Bosman, A., Romagnoli, C., Casagli, N., & Chiocci, F. L. (2021). Submarine and subaerial morphological changes associated with the 2014 eruption at Stromboli Island. *Remote Sensing*, *13*, 2043. https://doi.org/10.3390/rs13112043

Casalbore, D., Passeri, F., Tommasi, P., Verrucci, L., Bosman, A., Romagnoli, C., & Chiocci, F. L. (2020). Small-scale slope instability on the submarine flanks of insular volcanoes: The case-study of the Sciara del Fuoco slope (Stromboli). *International Journal of Earth Sciences*, *109*, 2643–2658. https://doi.org/10.1007/s00531-020-01853-5

Casalbore, D., Romagnoli, C., Bosman, A., Anzidei, M., & Chiocci, F. L. (2018). Coastal hazard due to submarine canyons in active insular volcanoes: Examples from Lipari Island (southern Tyrrhenian Sea). *Journal of Coastal Conservation*, *22*, 989–999. https://doi.org/10.1007/s11852-017-0549-x

Casalbore, D., Romagnoli, C., Bosman, A., & Chiocci, F. L. (2011). Potential tsunamigenic landslides at Stromboli Volcano (Italy): Insight from marine DEM analysis. *Geomorphology*, *126*, 42–50. https://doi.org/10.1016/j.geomorph.2010.10.026

Casalbore, D., Romagnoli, C., Pimentel, A., Quartau, R., Casas, D., Ercilla, G., et al. (2015). Volcanic, tectonic and mass-wasting processes offshore Terceira Island (Azores) revealed by high-resolution seafloor mapping. *Bulletin of Volcanology*, *77*, 24. https://doi.org/10.1007/s00445-015-0905-3

Casas, D., Chiocci, F., Casalbore, D., Ercilla, G., & de Urbina, J. O. (2016). Magnitude-frequency distribution of submarine landslides in the Gioia Basin (southern Tyrrhenian Sea). *Geo-Marine Letters*, *36*, 405–414. https://doi.org/10.1007/s00367-016-0458-2

Castello, B., Olivieri, M., & Selvaggi, G. (2007). Local and duration magnitude determination for the Italian earthquake catalog, 1981–2002. *Bulletin of the Seismological Society of America*, *97*, 128–139. https://doi.org/10.1785/0120050258

Chang, Y.-C., Mitchell, N. C., Hansteen, T. H., Schindlbeck-Belo, J. C., & Freundt, A. (2021). Volcaniclastic deposits and sedimentation processes around volcanic ocean islands: The central Azores. *Geological Society, London, Special Publications*, *520*, SP520. Geological SocietySpecial Publications. https://doi.org/10.1144/SP520-2021-62

Chaytor, J. D., Uri, S., Solow, A. R., & Andrews, B. D. (2009). Size distribution of submarine landslides along the US Atlantic margin. *Marine Geology*, *264*, 16–27. https://doi.org/10.1016/j.margeo.2008.08.007

Chiocci, F. L., & Casalbore, D. (2017). Unexpected fast rate of morphological evolution of geologically-active continental margins during Quaternary: Examples from selected areas in the Italian seas. *Marine and Petroleum Geology*, *82*, 154–162. https://doi.org/10.1016/j.marpetgeo.2017.01.025

Chiocci, F. L., Romagnoli, C., Casalbore, D., Sposato, A., Martorelli, E., Alonso, B., et al. (2013). Bathy-morphological setting of Terceira Island (Azores) after the FAIVI cruise. *Journal of Maps*, *9*, 590–595. https://doi.org/10.1080/17445647.2013.831381

Chiocci, F. L., Romagnoli, C., Tommasi, P., & Bosman, A. (2008). The Stromboli 2002 tsunamigenic submarine slide: Characteristics and possible failure mechanism. *Journal of Geophysical Research*, *113*. https://doi.org/10.1029/2007JB005172

CIVISA. (1998). *Boletim sismológico preliminar dos Açores*. (in Portuguese). Centro de Coordenação do Sistema de Vigilância Sismológica dos Açores, Instituto de Meteorologia and Azores University.

Clare, M., Chaytor, J., Dabson, O., Gamboa, D., Georgiopoulou, A., Eady, H., et al. (2018). A consistent global approach for the morphometric characterization of subaqueous landslides. *Geological Society, London, Special Publications*, *477*, SP477. https://doi.org/10.1144/sp477.15

Clauset, A., Shalizi, C. R., & Newman, M. E. (2009). Power-law distributions in empirical data. *SIAM Review*, *51*, 661–703. https://doi.org/10.1137/070710111

Costa, A. C. G., Hildenbrand, A., Marques, F. O., Sibrant, A. L. R., & Santos de Campos, A. (2015). Catastrophic flank collapses and slumping in Pico Island during the last 130 kyr (Pico-Faial ridge, Azores Triple Junction). *Journal of Volcanology and Geothermal Research*, *302*, 33–46. https://doi.org/10.1016/j.jvolgeores.2015.06.008

Crossen, R. S., & Endo, E. T. (1982). Focal mechanisms and locations of earthquakes in the vicinity of the 1975 Kalapana earthquake aftershock zone 1970-1979: Implications for tectonics of the south flank of Kilauea volcano, island of Hawaii. *Tectonics*, *1*, 495–542. https://doi.org/10.1029/TC001i006p00495

Cruz, J. V., & Silva, M. O. (2001). Hydrogeologic framework of Pico Island, Azores, Portugal. *Hydrogeology Journal*, *9*, 177–189. https://doi.org/10.1007/s100400000106

Das, R., Wason, H. R., & Sharma, M. L. (2011). Global regression relations for conversion of surface wave and body wave magnitudes to moment magnitude. *Natural Hazards*, *59*, 801–810. https://doi.org/10.1007/s11069-011-9796-6

De Lange, W., & Moon, V. (2004). Estimating earthquake and landslide tsunami hazard for the New Zealand coast. *Bulletin of the New Zealand Society for Earthquake Engineering*, *37*, 62–69. https://doi.org/10.5459/bnzsee.37.2.62-69

Dengler, A. T., Wilde, P., Noda, E. K., & Normark, W. R. (1984). Turbidity currents generated by Hurricane Iwa. *Geo-Marine Letters*, *4*, 5–11. https://doi.org/10.1007/BF02237967

Di Giacomo, D., Storchak, D., Safronova, N., Ozgo, P., Harris, J., Verney, R., & Bondár, I. (2014). A new ISC service: The bibliography of seismic events. *Seismological Research Letters*, *85*, 354–360. https://doi.org/10.1785/0220130143

Di Traglia, F., Nolesini, T., Solari, L., Ciampalini, A., Frodella, W., Steri, D., et al. (2018). Lava delta deformation as a proxy for submarine slope instability. *Earth and Planetary Science Letters*, *488*, 46–58. https://doi.org/10.1016/j.epsl.2018.01.038

Droxler, A. W., & Schlager, W. (1985). Glacial versus interglacial sedimentation rates and turbidite frequency in the Bahamas. *Geology*, *13*, 799–802. https://doi.org/10.1130/0091-7613(1985)13<799:gvisra>2.0.co;2

Federici, B., Bacino, F., Cosso, T., Poggi, P., Rebaudengo Landó, L., & Sguerso, D. (2006). Analisi del rischio tsunami applicata ad un tratto della costa Ligure. *MondoGIS*, *57*, 53–57.

Fine, I. V., Rabinovich, A. B., Bornhold, B. D., Thomson, R. E., & Kulikov, E. A. (2005). The Grand Banks landslide-generated tsunami of November 18, 1929: Preliminary analysis and numerical modeling. *Marine Geology*, *215*, 45–57. https://doi.org/10.1016/j.margeo.2004.11.007

Fornaciai, A., Favalli, M., & Nannipieri, L. (2019). Numerical simulation of the tsunamis generated by the Sciara del Fuoco landslides (Stromboli Island, Italy). *Scientific Reports*, *9*, 1–12. https://doi.org/10.1038/s41598-019-54949-7

Fornari, D. J., Moore, J. G., & Calk, L. (1979). A large submarine sand-rubble flow on Kilauea volcano, Hawaii. *Journal of Volcanology and Geothermal Research*, *5*, 239–256. https://doi.org/10.1016/0377-0273(79)90018-0

Frattini, P., & Crosta, G. B. (2013). The role of material properties and landscape morphology on landslide size distributions. *Earth and Planetary Science Letters*, *361*, 310–319. https://doi.org/10.1016/j.epsl.2012.10.029

Furumoto, A. S., & Kovach, R. L. (1979). The Kalapana earthquake and its relation to geothermal processes. *Physics of the Earth and Planetary Interiors*, *18*, 197–208. https://doi.org/10.1016/0031-9201(79)90114-6

Gabitov, R., Sadekov, A., Yapaskurt, V., Borrelli, C., Bychkov, A., Sabourin, K., & Perez-Huerta, A. (2019). Elemental uptake by calcite slowly grown from seawater solution: An in-situ study via depth profiling. *Frontiers in Earth Science*, *7*. https://doi.org/10.3389/feart.2019.00051

Garcia, M. O., Sherman, S. B., Moore, G. F., Goll, R., Popova-Goll, I., Natland, J. H., & Acton, G. (2006). Frequent landslides from Koolau Volcano: Results from ODP Hole 1223A. *Journal of Volcanology and Geothermal Research*, *151*, 251–268. https://doi.org/10.1016/j.jvolgeores.2005.07.035

Gaspar, J. L., Queiroz, G., Ferreira, T., Medeiros, A. R., Goulart, C., & Medeiros, J. (2015). Chapter 4 Earthquakes and volcanic eruptions in the Azores region: Geodynamic implications from major historical events and instrumental seismicity. *Geological Society, London, Memoirs*, *44*, 33–49. https://doi.org/10.1144/m44.4

Geist, E. L., Lynett, P. J., & Chaytor, J. D. (2009). Hydrodynamic modeling of tsunamis from the Currituck landslide. *Marine Geology*, *264*, 41–52. https://doi.org/10.1016/j.margeo.2008.09.005

Geist, E. L., & ten Brink, U. S. (2019). Offshore landslide hazard curves from mapped landslide size distributions. *Journal of Geophysical Research: Solid Earth*, *124*, 3320–3334. https://doi.org/10.1029/2018jb017236

Gràcia, E., Danobeitia, J., Vergés, J., & team, P. (2003). Mapping active faults offshore Portugal (36 N–38 N): Implications for seismic hazard assessment along the southwest Iberian margin. *Geology*, *31*, 83–86. https://doi.org/10.1130/0091-7613(2003)031<0083:MAFOPN>2.0.CO;2

Guzzetti, F., Ardizzone, F., Cardinali, M., Rossi, M., & Valigi, D. (2009). Landslide volumes and landslide mobilization rates in Umbria, central Italy. *Earth and Planetary Science Letters*, *279*, 222–229. https://doi.org/10.1016/j.epsl.2009.01.005

Haflidason, H., Lien, R., Sejrup, H. P., Forsberg, C. F., & Bryn, P. (2005). The dating and morphometry of the Storegga Slide. *Marine and Petroleum Geology*, *22*, 123–136. https://doi.org/10.1016/j.marpetgeo.2004.10.008

Hamilton, E. L. (1976). Shear-wave velocity versus depth in marine sediments: A review. *Geophysics*, *41*, 985–996. https://doi.org/10.1190/1.1440676

Hamilton, E. L., & Bachman, R. T. (1982). Sound velocity and related properties of marine sediments. *Journal of the Acoustical Society of America*, *72*, 1891–1904. https://doi.org/10.1121/1.388539

Hamilton, E. L., Shumway, G., Menard, H. W., & Shipek, C. J. (1956). Acoustic and other physical properties of shallow-sater sediments off San Diego. *Journal of the Acoustical Society of America*, *28*, 1–1. https://doi.org/10.1121/1.1908210

Hampton, M. A., Lee, H. J., & Locat, J. (1996). Submarine landslides. *Reviews of Geophysics*, *34*, 33–59. https://doi.org/10.1029/95RG03287

Heezen, B. C., & Ewing, M. (1952). Turbidity currents and submarine slumps, and the 1929 Grand Banks earthquake. *American Journal of Science*, *250*, 849–873. https://doi.org/10.2475/ajs.250.12.849

Hildenbrand, A., Madureira, P., Marques, F. O., Cruz, I., Henry, B., & Silva, P. (2008). Multi-stage evolution of a sub-aerial volcanic ridge over the last 1.3 Myr: S. Jorge Island, Azores Triple Junction. *Earth and Planetary Science Letters*, *273*, 289–298. https://doi.org/10.1016/j.epsl.2008.06.041

Hildenbrand, A., Marques, F. O., Catalão, J., Catita, C. M. S., & Costa, A. C. G. (2012). Large-scale active slump of the southeastern flank of Pico Island, Azores. *Geology*, *10*, 939–942. https://doi.org/10.1130/G33303.1

Hildenbrand, A., Weis, D., Madureira, P., & Marques, F. O. (2014). Recent plate re-organization at the Azores Triple Junction: Evidence from combined geochemical and geochronological data on Faial, S. Jorge and Terceira volcanic islands. *Lithos*, *210–211*, 27–39. https://doi.org/10.1016/j.lithos.2014.09.009

Hipólito, A., Madeira, J., Carmo, R., & Gaspar, J. L. (2014). Neotectonics of Graciosa Island (Azores): A contribution to seismic hazard assessment of a volcanic area in a complex geodynamic setting. *Annals of Geophysics*, *56*. https://doi.org/10.4401/ag-6222

Hu, G., Yan, T., Liu, Z., Vanneste, M., & Dong, L. (2009). Size distribution of submarine landslides along the middle continental slope of the East China Sea. *Journal of Ocean University of China*, *8*, 322–326. https://doi.org/10.1007/s11802-009-0322-3

Hunt, J. E., Wynn, R. B., Masson, D. G., Talling, P. J., & Teagle, D. A. H. (2011). Sedimentological and geochemical evidence for multistage failure of volcanic island landslides: A case study from Icod landslide on north Tenerife, Canary Islands. *Geochemistry, Geophysics, Geosystems*, *12*. https://doi.org/10.1029/2011gc003740

Hunt, J. E., Wynn, R. B., Talling, P. J., & Masson, D. G. (2013). Multistage collapse of eight western Canary Island landslides in the last 1.5 Ma: Sedimentological and geochemical evidence from subunits in submarine flow deposits. *Geochemistry, Geophysics, Geosystems*, *14*, 2159–2181. https://doi.org/10.1002/ggge.20138

Jibson, R. W. (2011). Methods for assessing the stability of slopes during earthquakes—A retrospective. *Engineering Geology*, *122*, 43–50. https://doi.org/10.1016/j.enggeo.2010.09.017

Joyner, W. B., & Boore, D. M. (1994). Methods for regression analysis of strong-motion data. *Bulletin of the Seismological Society of America*, *84*, 955–956.

Kadirioğlu, F. T., & Kartal, R. F. (2016). The new empirical magnitude conversion relations using an improved earthquake catalogue for Turkey and its near vicinity (1900-2012). *Turkish Journal of Earth Sciences*, *25*, 300–310. https://doi.org/10.3906/yer-1511-7

Kelfoun, K., Giachetti, T., & Labazuy, P. (2010). Landslide-generated tsunamis at Réunion Island. *Journal of Geophysical Research*, *115*. https://doi.org/10.1029/2009jf001381

Kelner, M., Migeon, S., Tric, E., Couboulex, F., Dano, A., Lebourg, T., & Taboada, A. (2016). Frequency and triggering of small-scale submarine landslides on decadal timescales: Analysis of 4D bathymetric data from the continental slope offshore Nice (France). *Marine Geology*, *379*, 281–297. https://doi.org/10.1016/j.margeo.2016.06.009

Klar, A., Aharonov, E., Kalderon-Asael, B., & Katz, O. (2011). Analytical and observational relations between landslide volume and surface area. *Journal of Geophysical Research*, *116*. https://doi.org/10.1029/2009JF001604

Krastel, S., Schmincke, H.-U., Jacobs, C. L., Rihm, R., Le Bas, T. P., & Alibes, B. (2001). Submarine landslides around the Canary Islands. *Journal of Geophysical Research*, *106*, 3977–3997. https://doi.org/10.1029/2000JB900413

Labazuy, P. (1996). Recurrent landsliding events on the submarine flank of Piton de la Fournaise volcano (Reunion Island). In W. J. McGuire, A. P. Jones, & J. Neuberg (Eds.), *Volcano instability on the Earth and other planets* (Vol. 110, pp. 295–306). London: Geological Society. https://doi.org/10.1144/GSL.SP.1996.110.01.23

Lee, H. J., Torresan, M. E., & McArthur, W. (1994). Stability of submerged slopes on the flanks of the Hawaiian Islands, a simplified approach. *Open-File Report*, *94–638*, 1–54. https://doi.org/10.2172/90387

Lipman, P. W., Normark, W. R., Moore, J. G., Wilson, J. B., & Gutmacher, C. E. (1988). The giant submarine Alika debris slide, Mauna Loa, Hawaii. *Journal of Geophysical Research*, *93*, 4279–4299. https://doi.org/10.1029/JB093iB05p04279

Lourenço, N., Miranda, J. M., Luis, J. F., Ribeiro, A., Victor, L. A. M., Madeira, J., & Needham, H. D. (1998). Morpho-tectonic analysis of the Azores volcanic plateau from a new bathymetric compilation of the area. *Marine Geophysical Researches*, *20*, 141–156. https://doi.org/10.1023/A:1004505401547

Macdonald, G. A. (1953). Pahoehoe, aa, and block lava. *American Journal of Science*, *251*, 169–191. https://doi.org/10.2475/ajs.251.3.169

Machado, F., Parsons, W. H., Richards, A. F., & Mulford, J. W. (1962). Capelinhos eruption of Fayal Volcano, Azores, 1957–1958. *Journal of Geophysical Research*, *67*, 3519–3529. https://doi.org/10.1029/JZ067i009p03519

Madeira, J. (1998). *Estudos de neotectónica nas ilhas do faial, Pico e S. Jorge: Uma contribuição para o conhecimento geodinâmico da junção tripla dos Açores* (Ph.D. dissertation). Lisbon University.

Madeira, J., & Brum da Silveira, A. (2003). Active tectonics and first paleoseismological results in Faial, Pico and S. Jorge islands (Azores, Portugal). *Annals of Geophysics*, *46*, 733–761. https://doi.org/10.4401/ag-3453

Madeira, J., Brum da Silveira, A., Hipólito, A., & Carmo, R. (2015). Chapter 3 Active tectonics in the central and eastern Azores islands along the Eurasia–Nubia boundary: A review. *Geological Society, London, Memoirs*, *44*, 15–32. https://doi.org/10.1144/m44.3

Maio, R., Estêvão, J. M. C., Ferreira, T. M., & Vicente, R. (2017). The seismic performance of stone masonry buildings in Faial Island and the relevance of implementing effective seismic strengthening policies. *Engineering Structures*, *141*, 41–58. https://doi.org/10.1016/j.engstruct.2017.03.009

Malamud, B. D., Turcotte, D. L., Guzzetti, F., & Reichenbach, P. (2004). Landslides, earthquakes, and erosion. *Earth and Planetary Science Letters*, *229*, 45–59. https://doi.org/10.1016/j.epsl.2004.10.018

Marinos, P., & Hoek, E. (2000). *GSI: A geologically friendly tool for rock mass strength estimation*. ISRM international symposium, International Society for Rock Mechanics and Rock Engineering.

Marques, F. O., Hildenbrand, A., & Hübscher, C. (2018). Evolution of a volcanic island on the shoulder of an oceanic rift and geodynamic implications: S. Jorge Island on the Terceira Rift, Azores Triple Junction. *Tectonophysics*, *738–739*, 41–50. https://doi.org/10.1016/j.tecto.2018.05.012

Masson, D., Le Bas, T., Grevemeyer, I., & Weinrebe, W. (2008). Flank collapse and large-scale landsliding in the Cape Verde Islands, off West Africa. *Geochemistry, Geophysics, Geosystems*, *9*. https://doi.org/10.1029/2008GC001983

Masson, D. G., Harbitz, C. B., Wynn, R. B., Pedersen, G., & Lovholt, F. (2006). Submarine landslides: Processes, triggers and hazard prediction. *Philosophical Transactions of the Royal Society*, *A364*, 2009–2039. https://doi.org/10.1098/rsta.2006.1810

Masson, D. G., Watts, A. B., Gee, M. J. R., Urgeles, R., Mitchell, N. C., Le Bas, T. P., & Canals, M. (2002). Slope failures on the flanks of the western Canary Islands. *Earth-Science Reviews*, *57*, 1–35. https://doi.org/10.1016/S0012-8252(01)00069-1

McAdoo, B. G., & Watts, P. (2004). Tsunami hazard from submarine landslides on the Oregon continental slope. *Marine Geology*, *203*, 235–245. https://doi.org/10.1016/S0025-3227(03)00307-4

McMurtry, G., Watts, P., Fryer, G., Smith, J., & Imamura, F. (2004). Giant landslides, mega-tsunamis, and paleo-sea level in the Hawaiian Islands. *Marine Geology*, *203*, 219–233. https://doi.org/10.1016/S0025-3227(03)00306-2

Menard, H. W. (1986). *Islands*. Scientific American Books.

Mitchell, N. C. (2003). Susceptibility of mid-ocean ridge volcanic islands and seamounts to large-scale landsliding. *Journal of Geophysical Research*, *108*. https://doi.org/10.1029/2002JB001997

Mitchell, N. C., Beier, C., Rosin, P., Quartau, R., & Tempera, F. (2008). Lava penetrating water: Submarine lava flows around the coasts of Pico Island, Azores. *Geochemistry, Geophysics, Geosystems*, *9*, Q03024. https://doi.org/10.1029/2007GC001725

Mitchell, N. C., Masson, D. G., Watts, A. B., Gee, M. J. R., & Urgeles, R. (2002). The morphology of the flanks of volcanic ocean islands: A comparative study of the Canary and Hawaiian hotspot islands. *Journal of Volcanology and Geothermal Research*, *115*, 83–107. https://doi.org/10.1016/S0377-0273(01)00310-9

Mitchell, N. C., Stretch, R., Oppenheimer, C., Kay, D., & Beier, C. (2012). Cone morphologies associated with shallow marine eruptions: East Pico Island, Azores. *Bulletin of Volcanology*, *74*, 2289–2300. https://doi.org/10.1007/s00445-012-0662-5

Mitchell, N. C., Stretch, R., Tempera, F., & Ligi, M. (2018). Volcanism in the Azores: A marine geophysical perspective. In C. Beier, & U. Küppers (Eds.), *Volcanoes of the Azores*. Springer. https://doi.org/10.1007/978-3-642-32226-6_7

Moore, J. G., Clague, D. A., Holcomb, R. T., Lipman, P. W., Normark, W. R., & Torresan, M. E. (1989). Prodigious submarine landslides on the Hawaiian Ridge. *Journal of Geophysical Research*, *94*, 17465–17484. https://doi.org/10.1029/jb094ib12p17465

Moore, J. G., Normark, W. R., & Holcomb, R. T. (1994). Giant Hawaiian landslides. *Annual Review of Earth and Planetary Sciences*, *22*, 119–144. https://doi.org/10.1146/annurev.ea.22.050194.001003

Nafisi, A., Montoya, B. M., & Evans, T. M. (2020). Shear Strength Envelopes of Biocemented Sands with Varying Particle Size and Cementation Level. *Journal of Geotechnical and Geoenvironmental Engineering*, *146*, 04020002. https://doi.org/10.1061/(ASCE)GT.1943-5606.0002201

Nunes, J. C., Forjaz, V. H., França, Z., & Fragoso, M. (2001). *Principais sismos destrutivos no arquipélago dos Açores—Uma revisão* (pp. 119–131). 5° Encontro Nacional de Sismologia e Engenharia Sísmica–SÍSMICA.

Nunes, J. C., & Ribeiro, E. (2001). *Caracterizaçao da sismicidade instrumental dos Açores no periodo 1950–1980*. SISMICA, Encontro Nacional de Sismologıa e Enghenaria Sısmica.

Ollier, G., Cochonat, P., Lenat, J. F., & Labazuy, P. (1998). Deep-sea volcaniclastic sedimentary systems: An example from La Fournaise volcano, Reunion Island, Indian Ocean. *Sedimentology*, *45*, 293–330. https://doi.org/10.1046/j.1365-3091.1998.0152e.x

Pacheco, J. (2002). *Processos associados ao desenvolvimento de erupções vulcânicas hidromagmáticas explosivas na ilha do Faial e sua interpretação numa perspectiva de avaliação do hazard e minimização do risco* (PhD thesis). Universidade dos Açores.

Pimentel, A., Pacheco, J., & Self, S. (2015). The ~1000-years BP explosive eruption of Caldeira Volcano (Faial, Azores): The first stage of incremental caldera formation. *Bulletin of Volcanology*, *77*, 1–26. https://doi.org/10.1007/s00445-015-0930-2

Pinto Ribeiro, L., Calvert, A., França, Z., Rodrigues, B., & Pinto de Abreu, M. (2010). *New $^{40}Ar/^{39}Ar$ and geochemical constraints on São Jorge island, Azores*. 1st International Workshop on Volcano Geology, at Madeira. Portugal.

Pratson, L. F., & Coakley, B. J. (1996). A model for the headward erosion of submarine canyons induced by downslope-eroding sediment flows. *The Geological Society of America Bulletin*, *108*, 225–234. https://doi.org/10.1130/0016-7606(1996)108<0225:AMFTHE>2.3.CO;2

Quartau, R., Hipólito, A., Romagnolii, C., Casalbore, D., Madeira, J., Tempera, F., et al. (2014). The morphology of insular shelves as a key for understanding the geological evolution of volcanic islands: Insights from Terceira Island (Azores). *Geochemistry, Geophysics, Geosystems*, *15*. https://doi.org/10.1002/2014GC005248

Quartau, R., Madeira, J., Mitchell, N. C., Tempera, F., Silva, P. F., & Brandão, F. (2015). The insular shelves of the Faial-Pico Ridge (Azores archipelago): A morphological record of its evolution. *Geochemistry, Geophysics, Geosystems*, *16*, 1401–1420. https://doi.org/10.1002/2015GC005733

Quartau, R., Ramalho, R. S., Madeira, J., Santos, R., Rodrigues, A., Roque, C., et al. (2018). Gravitational, erosional and depositional processes on volcanic ocean islands: Insights from the submarine morphology of Madeira Archipelago. *Earth and Planetary Science Letters*, *482*, 288–299. https://doi.org/10.1016/j.epsl.2017.11.003

Quartau, R., Tempera, F., Mitchell, N. C., Pinheiro, L. M., Duarte, H., Brito, P. O., et al. (2012). Morphology of Faial Island's shelf: The results of volcanic, erosional, depositional and mass-wasting processes. *Geochemistry, Geophysics, Geosystems*, *13*. https://doi.org/10.1029/2011GC003987

Quartau, R., Trenhaile, A. S., Mitchell, N. C., & Tempera, F. (2010). Development of volcanic insular shelves: Insights from observations and modelling of Faial Island in the Azores Archipelago. *Marine Geology*, *275*, 66–83. https://doi.org/10.1016/j.margeo.2010.04.008

Rahiman, T. I. H., & Pettinga, J. R. (2006). The offshore morpho-structure and tsunami sources of the Viti Levu Seismic Zone, southeast Viti Levu, Fiji. *Marine Geology*, *232*, 203–225. https://doi.org/10.1016/j.margeo.2006.07.007

Ramalho, R. S., Quartau, R., Trenhaile, A. S., Mitchell, N. C., Woodroffe, C. D., & Ávila, S. P. (2013). Coastal evolution on volcanic oceanic islands: A complex interplay between volcanism, erosion, sedimentation, sea-level change and biogenic production. *Earth-Science Reviews*, *127*, 140–170. https://doi.org/10.1016/j.earscirev.2013.10.007

Ramalho, R. S., Winckler, G., Madeira, J., Helffrich, G. R., Hipólito, A., Quartau, R., et al. (2015). Hazard potential of volcanic flank collapses raised by new megatsunami evidence. *Science Advances*, *1*, e1500456. https://doi.org/10.1126/sciadv.1500456

Ricchi, A., Quartau, R., Ramalho, R. S., Romagnoli, C., Casalbore, D., & Zhao, Z. (2020). Imprints of volcanic, erosional, depositional, tectonic and mass-wasting processes in the morphology of Santa Maria insular shelf. *Marine Geology*, *424*, 106163. https://doi.org/10.1016/j.margeo.2020.106163

Ryan, W. B. F., Carbotte, S. M., Coplan, J. O., O'Hara, S., Melkonian, A., Arko, R., et al. (2009). Global multi-resolution topography synthesis. *Geochemistry, Geophysics, Geosystems*, *10*, Q03014. https://doi.org/10.1029/2008GC002332

Sansone, F. J., & Smith, J. R. (2006). Rapid mass wasting following nearshore submarine volcanism on Kilauea volcano, Hawaii. *Journal of Volcanology and Geothermal Research*, *151*, 133–139. https://doi.org/10.1016/j.jvolgeores.2005.07.026

Santos, R., Quartau, R., da Silveira, A. B., Ramalho, R., & Rodrigues, A. (2019). Gravitational, erosional, sedimentary and volcanic processes on the submarine environment of Selvagens Islands (Madeira Archipelago, Portugal). *Marine Geology*, *415*, 105945. https://doi.org/10.1016/j.margeo.2019.05.004

Sawyer, D. E., & DeVore, J. R. (2015). Elevated shear strength of sediments on active margins: Evidence for seismic strengthening. *Geophysical Research Letters*, *42*(10), 10216–10221. https://doi.org/10.1002/2015GL066603

Scarth, A., & Tanguy, J.-C. (2001). *Volcanoes of Europe*. Harpenden.

Scholz, C. H. (1994). A reappraisal of large earthquake scaling. *Bulletin of the Seismological Society of America*, *84*, 215–218. https://doi.org/10.1016/0148-9062(94)90076-0

Scholz, C. H. (2002). *The mechanics of earthquakes and faulting*. Cambridge University Press. https://doi.org/10.1017/9781316681473

Schwab, W. C., Lee, H. J., Kayen, R. E., Quinterno, P. J., & Tate, G. B. (1988). Erosion and slope instability on Horizon Guyot, Mid-Pacific Mountains. *Geo-Marine Letters*, *8*, 1–10. https://doi.org/10.1007/BF02238000

Soule, S. A., Zoeller, M., & Parcheta, C. (2021). Submarine lava deltas of the 2018 eruption of Kīlauea volcano. *Bulletin of Volcanology*, *83*, 23. https://doi.org/10.1007/s00445-020-01424-1

Stein, R. S. (1999). The role of stress transfer in earthquake occurrence. *Nature*, *402*, 605–609. https://doi.org/10.1038/45144

Sun, Q., Alves, T. M., Lu, X., Chen, C., & Xie, X. (2018). True volumes of slope failure estimated from a quaternary mass-transport deposit in the northern South China Sea. *Geophysical Research Letters*, *45*, 2642–2651. https://doi.org/10.1002/2017gl076484

Tappin, D. R., Watts, P., McMurtry, G. M., Lafoy, Y., & Matsumoto, T. (2001). The Sissano, Papua New Guinea tsunami of July 1998—Offshore evidence of the source mechanism. *Marine Geology*, *175*, 1–23. https://doi.org/10.1016/S0025-3227(01)00131-1

ten Brink, U. S., Andrews, B., & Miller, N. (2016). Seismicity and sedimentation rate effects on submarine slope stability. *Geology*, *44*, 563–566. https://doi.org/10.1130/G37866.1

ten Brink, U. S., Barkan, R., Andrews, B. D., & Chaytor, J. D. (2009). Size distribution and failure initiation of submarine and subaerial landslides. *Earth and Planetary Science Letters*, *287*, 31–42. https://doi.org/10.1016/j.epsl.2009.07.031

ten Brink, U. S., Geist, E. L., & Andrews, B. D. (2006). Size distribution of submarine landslides and its implication to tsunami hazard in Puerto Rico. *Geophysical Research Letters*, *33*. https://doi.org/10.1029/2006gl026125

Tinti, S., Manucci, A., Pagnoni, G., Armigliato, A., & Zaniboni, F. (2005). The 30 December 2002 landslide-induced tsunamis in Stromboli: Sequence of events reconstructed from the eyewitness accounts. *Natural Hazards and Earth System Sciences*, *5*, 763–775. https://doi.org/10.5194/nhess-5-763-2005

Tommasi, P., Baldi, P., Chiocci, F. L., Coltelli, M., Marsella, M., & Romagnoli, C. (2008). Slope failures induced by the December 2002 eruption at Stromboli volcano. *Washington DC American Geophysical Union Geophysical Monograph Series* (Vol. 182, pp. 129–145). https://doi.org/10.1029/182GM12

Tucholke, B. E., Lin, J., Kleinrock, M. C., Tivey, M. A., Reed, T. B., Goff, J., & Jaroslow, G. E. (1997). Segmentation and crustal structure of the western Mid-Atlantic Ridge flank, 25°25′–27°10′N and 0–29 m.y. *Journal of Geophysical Research*, *102*, 10203–10223. https://doi.org/10.1029/96JB03896

Tucker, M. E., Carey, S. N., Sparks, R. S. J., Stinton, A., Leng, M., Robinson, L., et al. (2020). Carbonate crusts around volcanic islands: Composition, origin and their significance in slope stability. *Marine Geology*, *429*, 106320. https://doi.org/10.1016/j.margeo.2020.106320

Urgeles, R., & Camerlenghi, A. (2013). Submarine landslides of the Mediterranean Sea: Trigger mechanisms, dynamics, and frequency-magnitude distribution. *Journal of Geophysical Research: Earth Surface*, *118*, 2600–2618. https://doi.org/10.1002/2013jf002720

Varnes, D. J. (1978). Slope movement types and processes. In R. L. Schuster, & R. J. andKrizek (Eds.), *Landslides, analysis and control, special report 176* (pp. 11–33). National Academy of Sciences.

Walker, G. P. L. (1999). Volcanic rift zones and their intrusion swarms. *Journal of Volcanology and Geothermal Research*, *94*, 21–34. https://doi.org/10.1016/S0377-0273(99)00096-7

Watts, P., Grilli, S. T., Kirby, J. T., Fryer, G. J., & Tappin, D. R. (2003). Landslide tsunami case studies using a Boussinesq model and a fully nonlinear tsunami generation model. *Natural Hazards and Earth System Sciences*, *3*, 391–402. https://doi.org/10.5194/nhess-3-391-2003

Wessel, P., & Smith, W. H. F. (1991). Free software helps map and display data. *Eos, Transactions, American Geophysical Union*, *72*, 441. https://doi.org/10.1029/90eo00319

Wisshak, M., Berning, B., Jakobsen, J., & Freiwald, A. (2015). Temperate carbonate production: Biodiversity of calcareous epiliths from intertidal to bathyal depths (Azores). *Marine Biodiversity*, *45*, 87–112. https://doi.org/10.1007/s12526-014-0231-6

Wisshak, M., Form, A., Jakobsen, J., & Freiwald, A. (2010). Temperate carbonate cycling and water mass properties from intertidal to bathyal depths (Azores). *Biogeosciences*, *7*, 2379–2396. https://doi.org/10.5194/bg-7-2379-2010

Wu, T.-W., Suzuki, Y., Carlton, B., Harbitz, C., & Kopf, A. (2021). Effect of prior small to moderate seismic events on monotonic undrained shear strength of sand. *Soil Dynamics and Earthquake Engineering*, *141*, 106465. https://doi.org/10.1016/j.soildyn.2020.106465

Wynn, R., & Masson, D. (2003). Canary Islands landslides and tsunami generation: Can we use turbidite deposits to interpret landslide processes? In *Submarine mass movements and their consequences* (pp. 325–332). Springer. https://doi.org/10.1007/978-94-010-0093-2_36